AN ABSTRACT OF THE DISSERTATION OF

Jack T. Rundel for the degree of Doctor of Philosophy in Chemistry presented on January 16, 2008.

Title: Design, Fabrication and Application of a Microfluidic Nanofiltration Module for Separation and Purification of Macromolecules and Nanoparticles

Abstract approved:

_____

Vincent T. Remcho

A microfluidic nanofiltration module has been designed, fabricated and applied to the continuous-flow, pressure-driven, post-synthetic purification of macromolecules and nanoparticles via diafiltration using a commercially available organic solvent resistant nanofiltration membrane, STARMEM 122. This module will readily interface with other microscale components within a "nanofactory" for the rapid synthesis, purification and delivery of highly dispersed macromolecules and nanoparticles. The microfluidic nanofiltration module (MNM) fully integrates the membrane into an all-polymer format constructed of materials that are relatively inexpensive, chemically compatible with the targeted compounds and transmissive to visible light allowing optical monitoring of the system.

A molecular weight cutoff of 2.3 kDa was determined for the MNM using half-generation poly(amidoamine) dendrimer standards in a simulated post-synthetic mixture of 4 mM methyl acrylate in methanol. The membrane was also characterized within a macroscale test fixture (MTF), constructed of reusable parts that are easily disassembled for rapid replacement of the membrane. Rejections of 95% to 97% were observed in the MTF for triphenylphosphine (PPh_3) stabilized gold-eleven (Au_{11}) nanoparticle standards. Rejections of 12% to 58% were also observed for PPh_3, an anticipated post-synthetic byproduct. Purification via diafiltration of real-world post-synthetic Au_{11} mixtures was demonstrated in the MTF. Au_{11} rejections > 99% were observed along with expected decreases in PPh_3 concentrations. Stable permeances of 2 L m^{-2} h^{-1} bar^{-1} were also observed, comparable to those reported in the literature and claimed by the membrane manufacturer.

The purity of the Au_{11} final product was comparable to that of the crystalline Au_{11} standard purified by traditional means. These results suggest that a diafiltration system incorporating an organic solvent resistant nanofiltration membrane would be practical for rapid purification and high product recovery of gold nanoparticles in an organic solvent environment immediately downstream of a microreactor within a nanofactory architecture.

Design, Fabrication and Application of a Microfluidic Nanofiltration Module for Separation and Purification of Macromolecules and Nanoparticles

by
Jack T. Rundel

A DISSERTATION

submitted to

Oregon State University

in partial fulfillment of
the requirements for the
degree of

Doctor of Philosophy

Presented January 16, 2008
Commencement June 2008

Doctor of Philosophy dissertation of Jack T. Rundel presented on January 16, 2008.

APPROVED:

_____
Major Professor, representing Chemistry

_____
Chair of the Department of Chemistry

_____
Dean of the Graduate School

I understand that my dissertation will become part of the permanent collection of Oregon State University libraries. My signature below authorizes release of my dissertation to any reader upon request.

_____
Jack T. Rundel, Author

ACKNOWLEDGEMENTS

The author expresses sincere appreciation to the following:

Collaboration and Technical Support

Members of the Remcho Group, OSU

Members of the Paul Group, OSU

Members of the Chang Group, OSU

Members of the Ingle Group, OSU

Dr. Tom Plant, EECS, OSU

Todd Miller, MBI, OSU

Dr. Christine Pastorek, OSU

Michael Chan, OSU

Fabrication

Ted Hinke

Steve Etringer

Materials

Lallie McKenzie, UO

Jin Hyung Dae, OSU

Granwell Corporation of West Caldwell, NJ

Gentex Corporation of Zeeland, MI

Financial Support

W.M. Keck Foundation

Air Force Research Laboratories

TABLE OF CONTENTS

Page

LIST OF FIGURES

Figure Page

LIST OF FIGURES (Continued)

Figure Page

LIST OF FIGURES (Continued)

Figure Page

LIST OF APPENDIX FIGURES

Figure Page

LIST OF TABLES

DEDICATION

In memory of
M. Joan Rees Rundel,
my mother and first chemistry teacher,
and
Jack T. Rundel,
my father and inspiration for engineering,
for instilling in me a passion for learning,
a desire to help others
and the courage to follow my dreams.

Design, Fabrication and Application of a Microfluidic Nanofiltration Module for Separation and Purification of Macromolecules and Nanoparticles

1 Introduction

The overarching goal of this body of work is to develop a method of post-synthetic separation and purification to be incorporated within a "nanofactory" for the rapid production of macromolecules and nanoparticles. The method must be scalable to bench-top or industrial systems. The system should be composed of materials that are (1) relatively inexpensive, (2) can be shaped and joined using existing methods, (3) are chemically compatible with the targeted reagents and organic solvents, and (4) can withstand the expected temperature and pressure extremes. Optically transmissive materials are of particular interest due to the desire to (1) visually inspect the system in real-time on the macroscale for events such as bubble formation and cavity filling and (2) optically probe the system for concentrations of discrete species to evaluate reaction kinetics, concentration gradients and mass transport.

In response to these needs, a polymer format was chosen for the following reasons. Compared to metals and ceramics, polymers are *generally* less expensive and easier to machine and mold. Many polymers are commercially available in preformed sheets of uniform thickness and low surface roughness availing them to laminar architectures. Many polymers are transmissive in the visible spectrum. However, polymers are *generally* less compatible with organic solvent environments than commonly used metals and ceramics and

generally more limited regarding operating temperatures and mechanical strength.

Toward this goal, an all-polymer microfluidic nanofiltration module (MNM) has been designed, fabricated and applied toward the continuous-flow pressure-driven purification of macromolecules and nanoparticles via diafiltration using a commercially available organic solvent resistant nanofiltration membrane, STARMEM 122. Gasketing of the membrane and structural bonding of the amorphous polyethylene terephthalate (APET) hard-polymer laminae were realized through transmission laser welding. The membrane was also characterized in a macroscale test fixture (MTF), constructed of reusable parts that are easily disassembled for rapid replacement of the membrane.

Prior work has been done in related areas of interest. Dendrimers, highly monodisperse and spherically symmetric macromolecules, have been used previously to characterize pore size and Donnan exclusion effects in polymeric filtration membranes [1]. Organic solvent resistant nanofiltration membranes have been used on the macroscale for solvent exchange and homogeneous-catalyst recycling following organic syntheses [2]. On-chip purification, separation and preconcentration have been demonstrated with polymeric filtration membranes incorporated within microfluidic chips [3-6] as well as

filtering architectures fabricated in-situ [7, 8]. Microfluidic chips have been fabricated from PET substrates using thermal lamination techniques [9, 10]. To the author's knowledge this is the first report of incorporating a polymeric filtration membrane into a hard-polymer microfluidic device by transmission laser welding [11] and also the first reported purification of a post-synthetic gold nanoparticle mixture via nanofiltration.

1.1 Nanofactories

Nanofactories, one approach to atomically precise manufacturing [12], assemble products in the 0.1-100 nm size range by integrating microfluidic and micromechanical devices with component dimensions in the 0.1-100 μm size range. The characteristics of a nanofactory are analogous to those of a traditional chemical production factory: raw materials are combined in specified quantities with well-regulated environmental conditions; the resulting product is purified and concentrated; waste is minimized and handled responsibly; energy consumption and process times are kept to a minimum. In contrast to the traditional factory, phenomena such as surface tension, diffusive mixing and laminar flow dominate on the microscale with phenomena such as gravity, convective mixing and turbulent flow diminish in importance.

Of particular interest is the development of nanofactories for on-demand synthesis of nanoparticles [13-21] and macromolecules [22-24] in which

diffusion-limited parameters such as mixing, mass transport and heat exchange can be optimized for reduced residence times, more uniform reaction rates and increased product monodispersity. Potential advantages include increased safety, lower overall costs, increased product quality and greater research flexibility [25-28]. Safety could be enhanced by synthesis within a bench-top nanofactory by eliminating the need to transport experimental compounds with unknown toxicity, reducing potentially hazardous reaction volumes and obviating exposure routes to the user. Costs could be lowered through minimization of raw materials, energy consumption, and special storage needs. Product quality could improve by producing materials as needed, analogous to just-in-time manufacturing, thus reducing the possibility of degradation during transport and storage. Research could become more flexible with an integrated synthesis and purification system in which the user would easily program individual parameters such as residence time, mixing velocity or temperature thus bringing about automated multi-array production with high reproducibility.

1.2 Methods of Purification

The nanofactory would require methods of purifying the product. Ideally, these methods would support continuous throughput of the product stream in order to minimize handling losses and to maintain process consistency. Batch-mode methods of purification, in which the feed is delivered to the purification

system as a bolus of discrete volume, could achieve quasi-continuous throughput in a staggered mode of parallel units being fed in sequence. Continuous-mode methods of purification, in which the feed stream is not interrupted, would simply need to have the capacity to process the output volume of upstream components.

Some post-synthetic purifications can be accomplished through size discrimination since synthetic products are typically larger in mass and dimension than the starting materials and potential byproducts. Separation by size is of further importance to nanoparticles since their properties and applications are in many cases size-dependent. A number of batch-mode and continuous-mode methods have already been applied for purification and separation of nanoparticles and macromolecules.

1.2.1 Batch-Mode Purification

Many technologies have been developed over the decades for separation and purification methods that include some aspect of size-based discrimination. These can be classified as batch-mode if the feed is limited to discrete volumes. Several such methods have been developed in recent years for the purification and size-sorting of nanoparticles including: gel permeation chromatography (GPC) for carbon nanotubes [29-31], nanocrystalline CdSe [32] and gold nanoparticles [33-36]; GPC for shape-discrimination of rodlike

and spherical gold nanoparticles [36]; capillary electrophoresis [5, 37] and capillary zone electrophoresis [37] of gold nanoparticles; capillary gel electrophoresis and capillary electrochromatography of carbon nanotubes [5]; high-performance liquid chromatography of gold clusters [38, 39]; and ion exchange chromatography of gold clusters [40, 41].

1.2.2 Continuous-Mode Purification

Filtration, a well-known technique for size-based separation and purification, can be implemented in a continuous-mode format. The terminology and definitions of filtration vary somewhat from source to source but some generalities can be drawn. Filtration, in the broadest sense, is discrimination of a fluid mixture through a phase barrier and across a gradient. A familiar example is an aqueous suspension drawn through filter paper by gravity. However, fluids include both the liquid and gas phase. Phase barriers come in a variety of forms and are generally referred to as membranes. Gradients are usually, but not limited to, pressure and concentration. Through all of this, three terms remain well defined: the mixture to be filtered is the feed (f), that portion which passes through the membrane is the permeate (p), that which does not is the retentate (r).

An attempt can be made to characterize membranes as either porous or nonporous. A porous membrane has passages from one side to the other through which solvent, solutes and small particles can be transported via

convection or diffusion to become part of the permeate. Size discrimination is an obvious consequence of either fitting through the pore or not. A nonporous membrane is lacking such passages. Solvent and solute must dissolve into the membrane, diffuse across the membrane and dissolve out the other side in order to become part of the permeate. Since smaller solute molecules diffuse faster than larger solute molecules, size discrimination tends to be preserved. Keep in mind, on the nanoscale care must be taken when attempting to distinguish between molecule and nanoparticle, solution and suspension, pore space and interstitial space between polymer chains.

Yet another membrane characterization is based on electrostatic charge. A membrane with a surface charge will tend to reject species with similar charge but pass oppositely charged and neutral species. This effect is, of course, highly dependent upon pH of the solution and isoelectric points of solute species and the membrane itself. Since charge interactions are inversely proportional to the square of the distance, the surface of a small diameter pore will have a much greater influence on charged species transport than that of a larger diameter pore.

The performance of a filtration membrane with respect to a specific species is usually expressed in terms of rejection (R) and is often stated as percent rejection (Eq. 1). A rejection of 100% indicates that the membrane retained all

of a particular species. Whereas a rejection of 0% indicates that the membrane retained none of that species. Rejection is dependent upon many factors including concentration, pressure and flow conditions.

$$\text{rejection} = 1 - \frac{\text{permeate concentration}}{\text{retentate concentration}}$$

$$R = 1 - \frac{[p]}{[r]} \tag{1}$$

Filtration membranes are typically rated by a molecular weight cutoff (MWCO), defined as the molecular weight of a species that experiences 90% rejection. This means that the relative concentrations of that particular species in the retentate and permeate will be 10:1 as a result of the filtration. This value is meant to serve only as a rough estimate for predicting membrane performance with other species since it does not take into account possible variables such as molecular shape, charge effects or interactions such as adsorption, partitioning and swelling. Percent rejection and permeance are also highly dependent upon the solvent and solute conditions [42, 43]. This is thought to be due to solute/solvent, solute/membrane, and solvent/membrane interactions that are not easily predictable. As a result, nanofiltration membranes must be evaluated empirically for differing solvent systems and pressure ranges.

A combination of flow configurations can be realized depending upon the application needs or design restrictions (Fig. 1). Dead end flow, in which the feed flows orthogonal to the membrane surface, tends to be limited by issues such as concentration polarization and fouling of the membrane. Cross flow, in which the feed flows tangential to the membrane surface, is employed to minimize such effects. A sweep of solvent can be used to enhance transport in the permeate. Co-current refers to a sweep flowing in the same direction as the feed, whereas counter current is in the opposite direction. Diafiltration refers to methods in which the retentate is recirculated into the feed along with additional solvent in order to restore the feed volume.

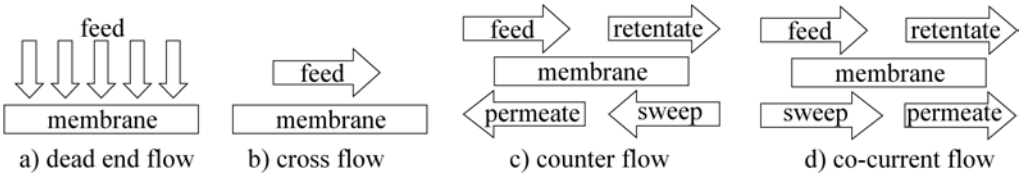

Figure 1: Schematics of flow configurations commonly used in filtration processes.

Demands for structural strength, chemical compatibility and surface charge have driven the development of a wide variety of materials and configurations far too numerous to detail here. Membrane architectures tend to fall neatly into two categories: symmetric (isotropic) and asymmetric (anisotropic). Symmetric membranes have a uniform structure with no orientation such as the simple fibrous filter paper example given above. Asymmetric membranes

consist of a thin, active layer providing selectivity bound to a thicker layer providing mechanical support.

There are several categories into which the spectrum of filtration has been divided (Eq. 2): microfiltration (MF), ultrafiltration (UF), nanofiltration (NF) and reverse osmosis (RO). Each is based *loosely* on a MWCO range expressed in Daltons (Da). Nanofiltration, in particular, has been defined as a "pressure-driven membrane-based separation process in which particles and dissolved macromolecules smaller than 2 nm are rejected" [44] and also as having a MWCO range of 200 to 1000 Da [45].

MF > 100,000 Da > **UF** > 1000 Da > **NF** > 100 Da > **RO** (2)

A further division in the classification of filtration methods has been observed in the response of solute rejection to applied transmembrane pressure. Rejections of solutes in microfiltration and ultrafiltration tend to decrease with increasing pressure while the converse is true for nanofiltration and reverse osmosis [46]. This can be seen as a consequence of whether convection or diffusion is the dominant mechanism of transport across the membrane [43, 47, 48]. When convection dominates the transport, solute and solvent fluxes are coupled. An increase in pressure increases the flux through the pores, which tends to lower solute rejection. When diffusion dominates the transport,

solvent and solute fluxes are uncoupled. An increase in pressure increases transport of smaller species more than larger species, which tends to increase solute rejection.

In nanofiltration processes, species with molecular weights similar to that of the solvent are expected to move across the membrane at roughly the same rate as the solvent thereby experiencing zero rejection [43]. In other words, the concentration of that particular species in the retentate is equal to the concentration in the permeate. The concentration of these small molecules that remain in the retentate can be decreased by iterative filtration steps in which the volume of the retentate is significantly reduced in every step and diluted with solvent between steps.

A theoretical treatment (Eq. 3) can be developed assuming R is constant (n = number of filtration steps; C = concentration; V = volume) [11]. By setting $V_f/V_r = 10$, we find that four filtration steps would be necessary to reduce the concentration of a species with 0% rejection by four orders of magnitude (Fig. 2).

$$\frac{mol_r}{mol_f} = \left[\left(\frac{V_f}{V_r} - 1\right)(1 - R) + 1\right]^{-n} \tag{3}$$

$$mol_f = mol_p + mol_r \tag{3a}$$

$$V_f C_f = V_p C_p + V_r C_r \tag{3b}$$

$$V_f = V_p + V_r \tag{3c}$$

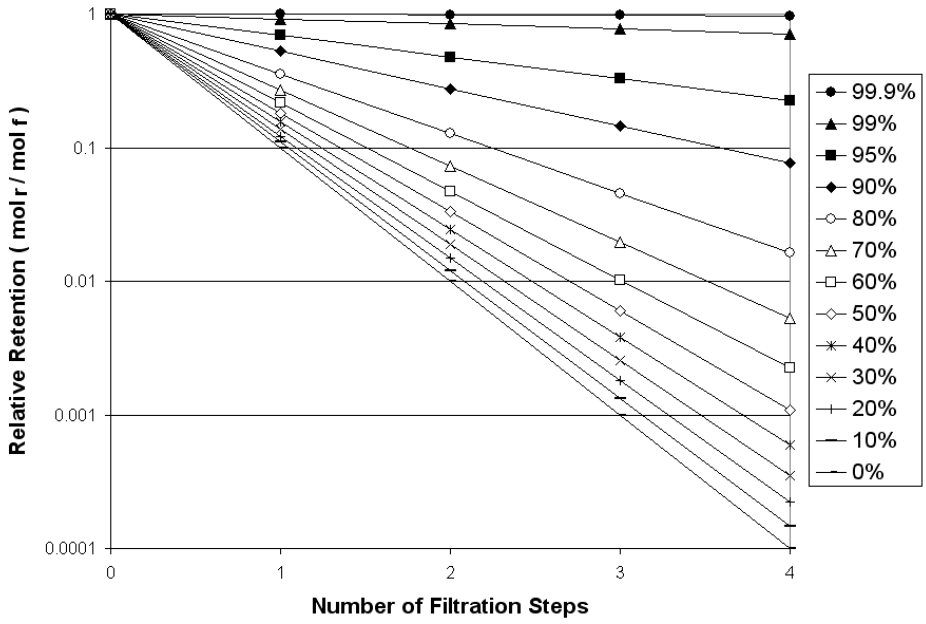

Figure 2: Relative retention of species following successive filtration steps. High rejection values (>99%) are needed to minimize product loss and low rejection values (<60%) allow significant removal of unwanted species from the product stream. Constant rates of rejection and a 10:1 feed volume to retentate volume are assumed. Series are given as percent rejection of species.

We also find that those same three filtration steps would reduce a species with 50% rejection by almost three orders of magnitude. In fact, rejections > 90% are necessary in order to achieve retentions > 10 % after four filtration steps.

In many synthetic processes, excess materials such as precursors, salts, monomers and emulsifiers must be removed in order to purify the desired product. Fortunately, most of these starting materials and byproducts are smaller in mass than the synthesized product. Recent work has demonstrated that filtration techniques can successfully be applied to purification and size fractionation of macromolecules and nanoparticles. Ultrafiltration methods

have been used for post-synthetic purification of aluminum, gold and polymer nanoparticles in aqueous environments [49-53]. Size fractionation of polydisperse gold nanoparticles has been demonstrated using both ultrafiltration and nanofiltration methods [51, 54].

Many product purification methods involve solvent exchange which introduces an additional solvent, many times a halogenated organic solvent, that would otherwise not be necessary in the overall production process. Many product concentration methods involve solvent removal, traditionally through evaporation. These methods are an economic burden because they are time consuming, labor intensive, energy intensive and environmentally unsound unless the solvents are handled properly. Nanofiltration offers an elegant alternative to these processes as a continuous-mode separation requiring relatively small amounts of energy to purify and concentrate a post-synthetic product stream without the need for additional solvents.

1.3 Macromolecules

A macromolecule is defined as "a molecule of high relative molecular mass, the structure of which essentially comprises the multiple repetition of units derived, actually or conceptually, from molecules of low relative molecular mass" [55]. In other words, a macromolecule is a polymer that exists as a

discrete molecular unit. There are well-known families of naturally occurring macromolecules including proteins, polysaccharides, and genetic material.

Dendrimers are a family of synthetic macromolecules characterized by highly branching structures radiating from a central core. Dendrimers are currently being studied for a variety of applications including targeted drug delivery in which the release of a drug is limited a specific organism or tissue type. One proposed targeted drug delivery concept involves encapsulating, thus isolating, a drug within a dendrimer shell and functionalizing the terminal groups of the dendrimer with tissue-specific antibodies. Upon injection, this drug delivery vehicle would be distributed *throughout* the body via the circulatory system, as would any other drug. However, upon encountering the targeted tissue the drug delivery vehicle would bind to the tissue via an antibody-antigen interaction, become immobilized and thereby concentrate. By applying some means of focused energy such as radiation or ultrasonication the dendrimer shell of the drug delivery vehicle would disintegrate thus releasing the drug in close proximity to the targeted tissue and reducing potential side effects.

One family of dendrimers, poly(amidoamine), PAMAM, has been studied for many years for such applications. In this work PAMAM was chosen as an exemplary macromolecule for rapid synthesis within a nanofactory. A brief synopsis of the divergent synthesis of PAMAM dendrimers with an ethylene

diamine (EDA) core is provided here in order to provide context for the nanofiltration application at hand. The details of the synthesis are provided in previous works [56, 57].

Divergent synthesis of PAMAM dendrimers consists of the iteration of two syntheses in which half-generations (Gx + 0.5) and full-generations (Gx), x = [-1, 0, 1,...], are built upon a core of the preceding generation. Illustrations of examples of these two syntheses are given in Figures 3 and 4.

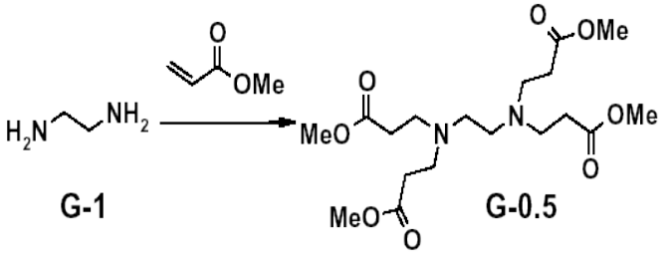

Figure 3: An illustration of the synthesis of half-generation PAMAM G-0.5. This is representative of the divergent synthesis of all half-generation PAMAM dendrimers.

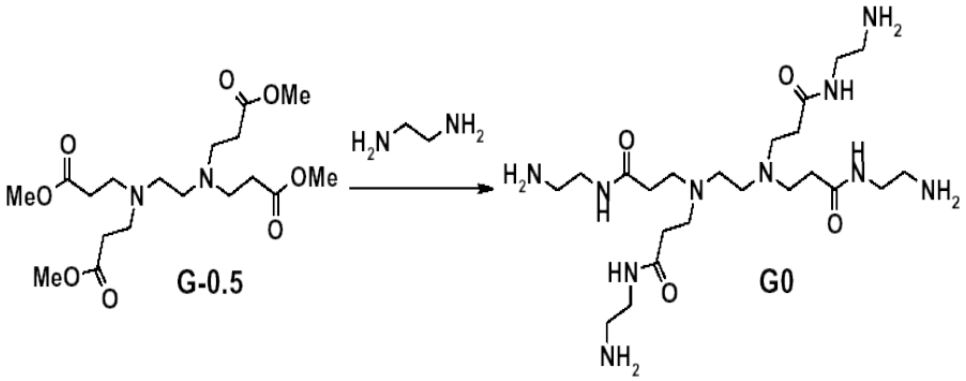

Figure 4: An illustration of the synthesis of full-generation PAMAM G0. This is representative of the divergent synthesis of all full-generation PAMAM dendrimers.

The first synthesis is the reaction of ethylene diamine (EDA), also known as G-1, with excess methyl acrylate (MA) to produce G-0.5 with four methyl ester-terminated branches. In the second synthesis, G-0.5 reacts with excess EDA to produce G0 with four amine-terminated branches. The cycle is repeated to achieve higher generations of ever increasing mass and size (Table 1). A dashed line is provided in the table to guide the eye to the division between low molecular weight species to be eliminated from the product stream and high molecular weight species to be retained in the product stream.

Table 1: Anticipated species in post-synthetic PAMAM product stream.

Component	Symbol	Mass	Fate in post-synthetic purification
methanol	MeOH	32	solvent and byproduct to be removed
ethylene diamine	EDA	60	excess reagent to be removed
methyl acrylate	MA	86	excess reagent to be removed
poly(amidoamine) generation -0.5	G-0.5	404	product to be retained
poly(amidoamine) generation 0	G0	517	product to be retained
poly(amidoamine) generation 0.5	G0.5	1205	product to be retained
poly(amidoamine) generation 1	G1	1430	product to be retained
poly(amidoamine) generation 1.5	G1.5	2807	product to be retained
poly(amidoamine) generation 2	G2	3256	product to be retained

In order to produce a monodisperse product though a sequence of iterated syntheses, excess reagent must be removed at the end of each synthesis. Any remaining EDA from full-generation syntheses or MA from half-generation syntheses will react in the next synthesis to produce G-0.5. If the G-0.5 is not removed from the product stream, it will react further thus creating a mixture of ever-increasing polydispersity.

A large difference in mass exists between the relatively small reagents and solvents as compared to the relatively large dendrimer products. This suggests that a size-based purification could effectively remove the excess reagents from a post-synthetic product stream thus preserving a high degree of monodispersity as the synthesis progresses. Another difference in mass is apparent *within* the half-generation or full-generation populations that constitutes more than a doubling in mass between successive dendrimers. This suggests that a size-based separation might improve the monodispersity of a post-synthetic product stream by removal of earlier generations and partially reacted side products should they arise.

The half-generation PAMAM dendrimers used in this study are carboxyl-terminated rather than the methyl ester-terminated dendrimers discussed in this section. The true half-generation dendrimers are not commercially available due to limited shelf life.

1.4 Nanoparticles

The term "nanoparticle" is a broad term that encompasses any particle with a least one dimension smaller than 100 nm. Nanoparticles typically have unique properties as a function of their size not observed in the bulk material. For example, semiconductor nanoparticles known as quantum dots exhibit a variety of luminescent properties as a function of their size.

The nanoparticle targeted in this study is gold-eleven (Au_{11}), a cluster of eleven gold atoms (d_{core} = 0.8 nm) stabilized by a shell of eight triphenylphosphine (PPh_3) ligands produced via reduction of $AuCl(PPh_3)$ with $NaBH_4$. The product, identified as ($Au_{11}(PPh_3)_8Cl_3$) via XPS, has been characterized using ^1H NMR, ^{31}P NMR, UV-vis, and TEM [51].

The masses of known species involved in the reaction are given in Table 2. A dashed line is provided in the table to guide the eye to the division between low molecular weight species to be eliminated from the product stream and high molecular weight species to be retained in the product stream. The chemical equation for the synthesis reaction is shown (Eq. 4) along with the caveat that the exact fate of many of the species, shown in italics, is not yet known.

Table 2: Anticipated species in a post-synthetic Au_{11} product stream.

Component	Symbol	Mass	Fate in post-synthetic purification
sodium borohydride	$NaBH_4$	38	reducing agent to be removed
ethanol	EtOH	46	50% of solvent volume
tetrahydrofuran	THF	72	50% of solvent volume
triphenyl phosphine	PPh_3	262	side product to be removed
chloro(triphenylphosphine)gold(I)	$AuCl(PPh_3)$	495	precursor to be removed
gold eleven	$Au_{11}(PPh_3)_8Cl_3$	4371	product to be retained

$$11\,AuCl(PPh_3) + 11\,NaBH_4 \rightarrow Au_{11}(PPh_3)_8Cl_3 + 3\,PPh_3 + 8\,\mathit{Cl} + 11\,\mathit{Na} + 11\,\mathit{B} + 44\,\mathit{H} \quad (4)$$

Gas is evolved in the reaction and allowed to escape to atmosphere. This is suspected to be H_2 but might also contain BH_3. PPh_3 is known to slowly oxidize to $OPPh_3$. The complex PPh_3-BH_3 has been produced via other synthetic methods involving PPh_3 and $NaBH_4$ in THF [58]. It is also been observed that the post-synthetic mixture will react further to form other nanoparticles and eventually plate out elemental gold.

Conventional purification of the resulting Au_{11} product involves precipitating the product in a non-polar organic solvent, recovering the solid by filtration through a sintered frit, redissolving the solid in a halogenated organic solvent and recrystallizing the product via solvent evaporation. The entire process takes about 24-hours and does not adequately remove all the reaction byproducts.

For the purposes of this study it is assumed that: (1) the synthetic reaction goes to completion, exhausting the supply of the reducing agent ($NaBH_4$) and the gold precursor ($AuCl(PPh_3)$); (2) the solvents (THF and EtOH) move across the membrane at the same rate, therefore the solvent composition remains the same throughout; (3) electrostatic charge effects are negligible; (4) PPh_3 does not complex or oxidize; and (5) the relatively low-weight spectator species (Na, Cl, B, H) experience 0% rejection and therefore occur in equal concentrations in the feed, retentate and permeate of a given filtration step.

Based on these assumptions, removal of PPh_3 and retention of Au_{11} represent the crux of the purification. If PPh_3 experiences low rejection (<60%), it will be removed from the product stream and all the other smaller byproducts of the reaction will be removed to an even greater extent. If Au_{11} experiences high rejection (>99%), it will be retained in the product stream throughout the process.

2 Materials and Methods

2.1 Introduction

Selection of materials and methods is a critical step in any investigation. In addressing this particular research question the most pressing materials constraint is the choice to operate a fully polymeric system in organic solvent environments. Fortunately, commercially available nanofiltration membranes have been developed in recent years that are resistant to a variety of organic solvents. Also, a wide variety of hard-polymer substrate candidates are available that are inexpensive, relatively strong, and transmissive in the visible. However, identifying one that can be shaped and bonded to form a microfluidic device *and* withstand a variety of organic solvents presents a challenge.

2.2 STARMEM 122

The organic solvent resistant nanofiltration membrane, STARMEM 122 (Membrane Extraction Technologies, London, UK), used in this study is of polyimide construction compatible with a wide range of organic solvents including alcohols, alkanes, aromatics, ethers and ketones. The manufacturer states that it has a MWCO = 220 Da for normal alkanes in toluene at 55 bar with a permeance of 0.5 L m^{-2} h^{-1} bar^{-1}. It is conveniently available in 8.5 in. x

11 in. dry sheets that can easily be cut with scissors and has no special storage or handling needs. It comes impregnated with stabilizing oil to be flushed out during a preconditioning step prior to use and discarded. Once wetted, the membrane must be kept wet in order to maintain performance. Other STARMEM membranes are available with a MWCO range of 200-400 Da. All are meant to be operated at pressures of 30-60 bar. They are considered to be nonporous with solution-diffusion models best predicting their performance [43].

STARMEM 122 is an asymmetric membrane composed of a dense yellow layer, providing selectivity, bound to a more porous layer, providing mechanical support. These layers can be easily delaminated by gently peeling them apart. In this body of work, the selective layer is referred to SMA (for "STARMEM active") while the supporting layer is referred to as SMB (for "STARMEM backing"). A separate, thicker and more porous fibrous membrane is provided with each sheet of STARMEM 122 to be used for additional mechanical support if needed. SMA and SMB are each 100 μm thick whereas the fibrous membrane is 250 μm thick.

The components of the STARMEM 122 system (SMA, SMB, and the fibrous membrane) were analyzed individually by differential scanning calorimetry

(DSC) and thermogravimetric analysis (TGA) in an attempt to ascertain more details of their respective compositions (Figs. 5 and 6).

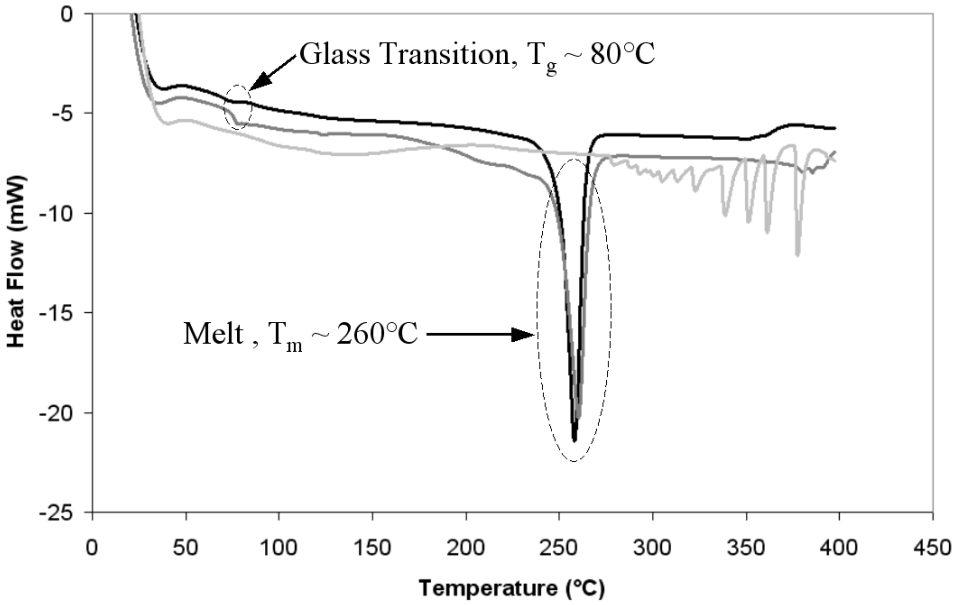

Figure 5: Differential scanning calorimetry of STARMEM 122 components. Legend: black = SMB, dark gray = fibrous membrane, light gray = SMA. The SMB and fibrous membrane are likely composed of the same material; perhaps polyethylene terephthalate (PET) (T_g = 70°C to 80°C, T_m = 245°C to 265°C).

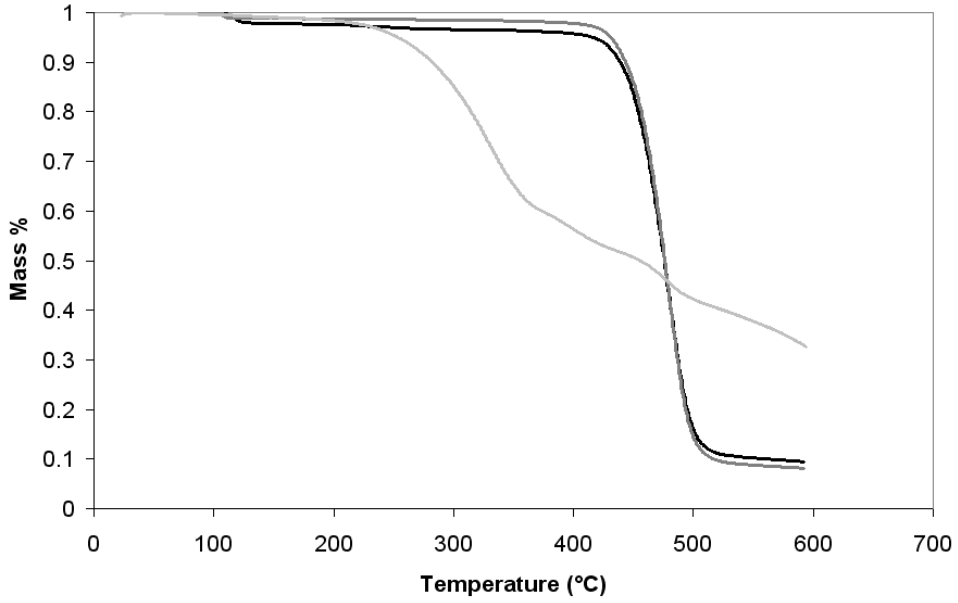

Figure 6: Thermogravimetric analysis of STARMEM 122 components. Legend: black = SMB, dark gray = fibrous membrane, light gray = SMA. The backing layer and fibrous layer share similar composition.

SMB and the fibrous backing are thought to be composed of very similar materials, mostly polyethylene terephthalate (PET). They share the same glass transition temperature (T_g = 80°C) and the same melt temperature (T_m = 260°C). Both of these properties are similar to those reported for PET (T_g = 70°C to 80°C); (T_m = 245°C to 265°C). PET is also known to be hygroscopic, which might explain the slight weight loss occurring just above 100°C in the TGA of both the SMB and fibrous membrane of -4% and -2% respectively. The decomposition of both samples occurs between 400°C and 500°C but is not indicative of any particular polymer material. Both materials contain approximately 10% non-organic content as seen in the mass fraction that remains above 500°C.

The composition of SMA is not so easily surmised. This is understandable since the membrane is impregnated with oil and probably composed of a mixture of polymers. No distinct T_g or T_m is evident in the DSC of SMA. However, this does correlate somewhat with the manufacturer's claim that the SMA has a polyimide composition. Polyimide is reported to have no T_g and a T_m = 310°C to 365°C. The noise seen in the DSC of SMA starting at about 275°C might be obscuring an indicative T_m. This noisy region in the DSC is likely attributable to the steady loss of mass shown in the TGA of SMA starting at ~250°C. This is probably a result of the volatilization of the impregnating oils used to stabilize the membrane during dry storage.

2.3 Clearweld and Transmission Laser Welding

Clearweld (Gentex, Zeeland, MI) is a commercially available liquid used for transmission laser welding of polymers that are themselves transmissive in the near infrared (NIR). Clearweld consists of a proprietary molecule that absorbs NIR dissolved in a volatile organic solvent. This solution is deposited onto a surface to be welded by any appropriate means after which the volatile content rapidly evaporates leaving behind a thin film of the absorbing molecule with a green tint. A second polymer substrate is then brought into contact with the thin film. Upon exposure to NIR of sufficient power density the thin film heats

and melts the polymer substrates. Assuming miscibility of the polymer substrates, sufficient clamping pressure and good contact between the surfaces, a clear weld will form upon cooling. The particular formula of Clearweld used in this study, LD120B, contains acetone as its organic solvent. Measurements made in-house of 10^{-3} M of LD120B in acetone show a broad absorbance band (FWHM = 300 nm) in the NIR with a maximum at 960 nm. A narrower absorbance band (FWHM = 60) in the visible with a maximum at 420 nm and a magnitude that is 87% of that in the NIR.

2.4 Reagents and Materials

All of the remaining materials used and tested for use in this study are listed below in the appropriate general category.

Organic Liquids

- methanol (MeOH) (HPLC grade, Merck, Whitehouse Station, NJ)
- ethanol (EtOH) (100%, Aaper Alcohol, Shelbyville, KY)
- methyl acrylate (MA) (>99.0%, Sigma-Aldrich, St. Louis, MO)
- ethylene diamine (EDA) (Fisher, Pittsburgh, PA)
- glacial acetic acid (HAc) (Fisher)
- tetrahydrofuran (THF) (HPLC grade, Merck)
- dichloromethane (DCM) (HPLC grade, Mallinckrodt Baker, Phillipsburg, NJ)

Species Targeted for Filtration

- Rhodamine B (RhB) (LC6100, Coherent, Santa Clara, CA)
- poly(amidoamine) dendrimers (PAMAM, EDA core) (Sigma-Aldrich)
- triphenylphosphine (PPh_3) (99%, Sigma-Aldrich)
- PPh_3 stabilized gold-eleven (Au_{11})
    - Crystalline standards (Lallie McKenzie, UO, Eugene, OR)
    - Post-synthetic samples (Jin Hyung Dae, OSU, Corvallis, OR)

Hard-polymer Substrates

- polysulfone (PSU) (K-Mac Plastics, Wyoming, MI)
- polyvinylchoride (PVC) (Hytek Plastics, Corvallis, OR)
- polyethylene terephthalate (PET) (McMaster, Los Angeles, CA)
- amorphous PET (APET) (ALRO Plastics, Jackson, MI)
- PET with cyclohexane dimethanol copolymer (PETG) (McMaster)
- polyetherimide (PEI) (McMaster)
- polycarbonate (PC) (McMaster)
- polyether ether ketone (PEEK) (McMaster)
- polymethylmethacrylate (PMMA) (McMaster)

Elastomeric Gasketing Material

- polydimethylsiloxane (PDMS) (Dow Corning, Midland, MI)
- Viton O-rings (O-Rings West, Seattle WA).
- ethylene polypropylene copolymer O-rings (EPDM) (O-Rings West)
- PTFE-encapsulated Viton O-ring (O-Rings West)

2.5 Materials Compatibility

A survey of possible polymer candidates was conducted to identify materials that would not be attacked by the various organic solvents [11]. The ideal hard-polymer substrate would be: (1) thermoplastic for future embossing of microfeatures; (2) transmissive in the visible for optical monitoring; (3) transmissive in the near infrared (NIR) for transmission laser welding; (4) chemically resistant to the various organic solvent environments; and (5) machinable with minimal burring to allow for rapid prototyping in the design phase. The ideal gasketing material would be: (1) an elastomeric polymer with low hardness; (2) inexpensive and readily available in the required dimensions; and (3) chemically resistant to the various organic solvent environments. Hard-polymers selected for study included APET, PSU, PVC, PET, PETG, PEI, PC, PEEK, PTFE and PMMA. Elastomeric polymers selected for study included PDMS, Viton, and EPDM. The membrane materials SMA and SMB were also studied for solvent compatibility. Polymer samples available in sheets were cut to size at 0.25 in. x 1.5 in. with thicknesses depending on substrate source. Sections cut from O-rings were used for testing of Viton and EPDM.

For PAMAM testing, a dilution scheme of 100%, 10% and 1% v/v in MeOH of EDA, MA and HAc was used. For Au_{11} testing, the same 100%, 10% and 1% v/v dilution scheme was applied to THF and DCM in EtOH. An additional

dilution scheme of 90% to 20% at 10% increments was applied to THF in EtOH on select polymers when greater resolution was needed surrounding the targeted 50% v/v THF/EtOH. All solutions were prepared in bulk and dispensed as 2.0 ml aliquots into 4 ml glass vials. Samples of each polymer were massed and placed in the respective solvent environments. A control for each polymer type, not exposed to the solvent environment, was left at ambient atmospheric conditions in a sealed plastic bag for the duration of the test.

After 24 hours of exposure each sample was removed from the solvent environment, rinsed with either MeOH or EtOH, and blown dry with N_2 gas to remove any residual solvent. The samples were then weighed, placed in rough vacuum for 10 minutes and weighed again. The net loss or gain in mass was then calculated. The quantitative performances of the materials tested are given in Appendix A. Visual inspection of the polymer samples provided qualitative observations including haze, swelling, discoloration and etching. Each sample was then returned to its respective solvent environment for long-term exposure observations.

SMA was found to be incompatible with EDA at any concentration and compatible with MA at lower concentrations (<10%). As a result, the PAMAM study was limited to half-generations only.

For use in half-generation PAMAM filtration, APET, PET, PSU, PEEK, PTFE, and EPDM were selected as suitable materials at low MA concentrations. PMMA, PC, PEI, PVC, PETG, PDMS and Viton were rejected due to excessive changes in mass due either to solvent uptake or dissolution of the polymer. PVC, PETG and PDMS also showed unacceptable discoloration and haze.

For use in Au_{11} filtration, only the set of polymers suitable for PAMAM filtration were chosen for compatibility testing. All were selected for use in 50% THF with the exception of PSU.

PET was selected as the best overall candidate. Although transparent PET is widely available in sheets thinner than 1 mm and ubiquitous as beverage containers and food packaging, larger thicknesses are only available in the naturally white-opaque form due to its semi-crystalline structure. As a result, PSU was selected as the thick hard-polymer substrate for use in PAMAM macroscale filtration in order to preserve some degree of transparency for process monitoring. Opaque PET was selected as the thick hard-polymer substrate for use in Au_{11} macroscale filtration because there was simply no other suitable candidate. APET, available in optically transparent 1 mm sheets, was selected as the thin hard-polymer substrate for both PAMAM and Au_{11} microscale filtration.

2.6 Macroscale Test Fixture (MTF)

A macroscale test fixture (MTF) was designed for initial characterization of the STARMEM 122 membrane and to demonstrate macroscale performance of dead-end flow [11]. The MTF was constructed of reusable parts that could be easily disassembled in order to replace the membrane whenever necessary. The fixture was designed to provide an effective membrane surface area of 10 cm^2 and a channel height above the membrane of 0.25 cm resulting in a retentate volume of 2.5 mL.

Two MTF units were fabricated for use in this study. The MTF used for PAMAM testing was constructed of PSU and the MTF used for Au11 testing was constructed of opaque PET. In both cases, hard-polymer 0.5 in. stock was machined using a shop lathe and mill to form the upper and lower components (Fig. 7).

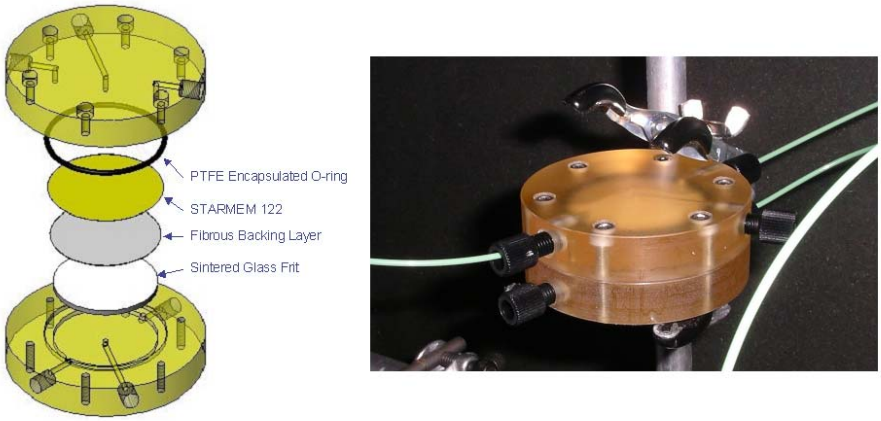

Figure 7: The macroscale test fixture (MTF). A SolidWorks rendering of the MTF allowing dead end flow testing of the membrane up to 7 bar (left panel). Macroscale test fixture is shown in use with fluidic interface (right panel).

Three fluidic ports were placed in both the upper and lower components of the MTF. The two ports near the perimeter of the circular channel permitted filling and emptying of the channel in the upper component during procedures such as burping trapped air, recovering retentate and rinsing with solvent. The same was not true for the lower component due to the high porosity and resulting surface tension of the sintered frit that filled the channel. The ports at the centers of the circular channels served as the inlet for the feed in the upper component and outlet for the permeate in the lower component.

Gasketing was achieved with a PTFE-encapsulated Viton O-ring and mechanical support for the membrane was provided by a sintered glass frit. The membrane and backing material were cut to size with a cylindrical stainless steel punch fabricated specifically for that purpose. The fluidic

interface to the MTF was comprised of ¼ in.-28 Delrin fittings, Tefzel ferrules and 0.015 in. I.D. x 1/16 in. O.D. PEEK tubing (Upchurch Scientific).
When fully assembled, the inner faces of the upper and lower components met ensuring a reproducible volume and uniform height of the product stream channel.

2.7 Microfluidic Nanofiltration Module (MNM)

A microfluidic nanofiltration module (MNM) was designed and fabricated for cross current flow in the product stream channel and either co-current or counter current flow in the permeate stream channel (Fig. 8) [11]. However, in this body of work the MNM was operated in a cross flow geometry in order to sample the permeate without dilution from a sweep stream and thereby more accurately assess the performance of the membrane.

A fluidic interface fixture for the MNM was designed and fabricated to register the MNM inlets and outlets and to provide clamping support for the O-ring gaskets (Fig. 8). The fluidic interface was comprised of Nanoport assemblies to accept 0.015 in. I.D. x 1/16 in. O.D. PEEK tubing (Upchurch Scientific) and M1x4 EPDM O-rings to provide solvent resistant gasketing of the Nanoports. The fixture was constructed from 0.5 in. PC and clamped using stainless steel machine screws.

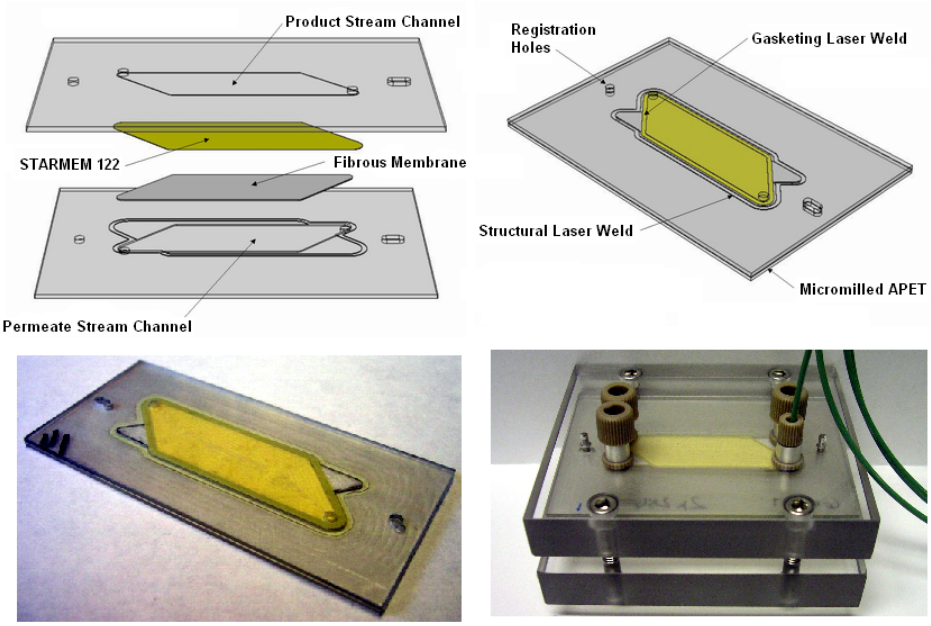

Figure 8: The microfluidic nanofiltration module (MNM). A SolidWorks rendering of an exploded view (top left) and fully assembled (top right). Photographs of the microfluidic nanofiltration module (bottom left) and the microfluidic nanofiltration module mounted in the fluidic interface (bottom right).

Mechanical reinforcement of both sides of the MNM was provided by a 1/8 in. glass shim inserted between the fixture and the MNM in order to counteract a ballooning of the APET substrate observed during testing. Each slab was secured in place by two sets of ¼ in.-28 Super Flangless nuts and ferrules (Upchurch Scientific).

2.7.1 Micromilling

The product stream channel was milled to a 100 μm depth in 1 mm thick APET with an inlet for the feed and an outlet for the retentate. A permeate stream channel was milled to a depth of 250 μm into a second 1 mm thick

APET substrate with an inlet for the sweep and an outlet for the permeate. The permeate channel was completely filled by a fibrous membrane thus providing mechanical support for the membrane while preserving a flow path for the sweep and permeate. The resulting geometry provided approximately 4 cm^2 of effective membrane surface area.

All milling was performed on a Tool Crafter mill (CMS CNC, Laguna Hills, CA). Deburring was done manually using a variety of tools as needed including a thin stainless steel shim as a scraper, a soft-bristle brush, a fine pick and paper as an abrasive surface.

2.7.2 Clearweld Deposition and Transmission Laser Welding

In order to define the transmission laser weld line, a thin film of Clearweld was deposited onto the micromilled APET substrates along the perimeters of the product stream channel and the permeate stream channel. This was accomplished using a thermal ink jet technology that achieved uniform deposition of the fluid at feature widths ranging from 100 to 1000 μm. Studies were also conducted using a felt pen to deposit the Clearweld fluid. However, this technique did not provide adequate precision in the placement, width and density of the Clearweld line resulting in inconsistent weld quality.

Laser welding was performed with an IRAM 300 (Branson Ultrasonics, Danbury, CT) laser welding system retrofitted with a 940 nm vertical stack diode array dispersed in a 1.8 x 80 mm swath. For the membrane-to-APET weld, the diode array was supplied with a current of 40.0 A resulting in 195 W of photonic power. For the APET-to-APET weld the diode array was supplied with a current of 50.0 A resulting in 275 W of photonic power. Both welds were realized with a scan speed of 10 mm/s and a clamping force of 1.3 kN (4.1 bar on a 64 mm diameter air cylinder).

2.7.3 Gasketing Weld

The STARMEM 122 membrane sheet, cut with scissors into a rectangular blank with dimensions larger than the product stream channel, was laser welded to the APET substrate with the active layer of the membrane toward the product stream channel. This formed a gasketing seal between the membrane and the APET substrate around the entire perimeter of the product stream channel. The excess nanofiltration membrane and the backing layer of the gasketed membrane were then removed in a single step by pulling the edge of the excess membrane away from the substrate surface while applying force tangentially along the weld line with a razor blade. This peeling process defined a clean edge along the outside of the gasketing weld and delaminated the SMB leaving only the SMA welded to the APET.

2.7.4 Fibrous Membrane

The fibrous membrane was cut to size via laser ablation using an ESI 5330 (Electro Scientific Industries, Portland, OR) laser trimming system tool (wavelength = 355 nm, spot size = 40 μm, power = 6.0 W, velocity = 30 mm/s, and rep rate = 30 kHz). The tool path for the cut matched the dimensions of the perimeter of the permeate channel with a tool offset of one beam radius to the inside. This resulted in a fibrous membrane that was smaller than the permeate channel by approximately 100 μm (~ 0.004 in.) on each edge. The fibrous membrane then fit snugly in the permeate channel without any pressure needed to position it or hold it in place.

2.7.5 Structural Weld

The product stream channel/SMA assembly was then welded onto the permeate stream channel/fibrous membrane assembly along a raised feature that defines the perimeter of the permeate stream channel. This raised feature serves several purposes in determining the final dimensions and strength of the device. First of all, the raised feature localizes the clamping pressure during assembly: the contact between the product stream channel part and the permeate stream channel part is limited to the top surface of the raised feature ensuring that the entire perimeter of the raised feature is in contact with the surface of the product stream channel part, a requirement for achieving a good

weld. Secondly, the raised feature is crushed under the clamping force as it melts: the crush is only stopped when the top of the permeate stream channel and nested fibrous membrane are incident upon the back of the nanofiltration membrane ensuring that an open channel does not exist either above or below the fibrous membrane. Thirdly, part of the melt volume flows into any voids between the edge of the nanofiltration membrane and the edge of the raised feature minimizing the dead space in the permeate stream channel and reducing the possibility of an open channel flow along the edge of the permeate stream channel. Finally, part of the melt volume flows into the edge of the fibrous membrane itself anchoring the fibrous membrane in place. In order to achieve a uniform structural weld, a crush zone with a height of 50 μm and width of 1 mm was milled along the entire perimeter of the permeate stream channel.

2.7.6 Registration Fixture

A registration fixture was used to align the parts during Clearweld deposition and welding (Fig. 9). Registration pins protrude out of the surface of a ground aluminum substrate. The pins are backed by compression springs allowing them to be pressed flush with the surface of the fixture. This design ensures that the pins will not obstruct the quartz plate that provides clamping pressure to the assembly during welding.

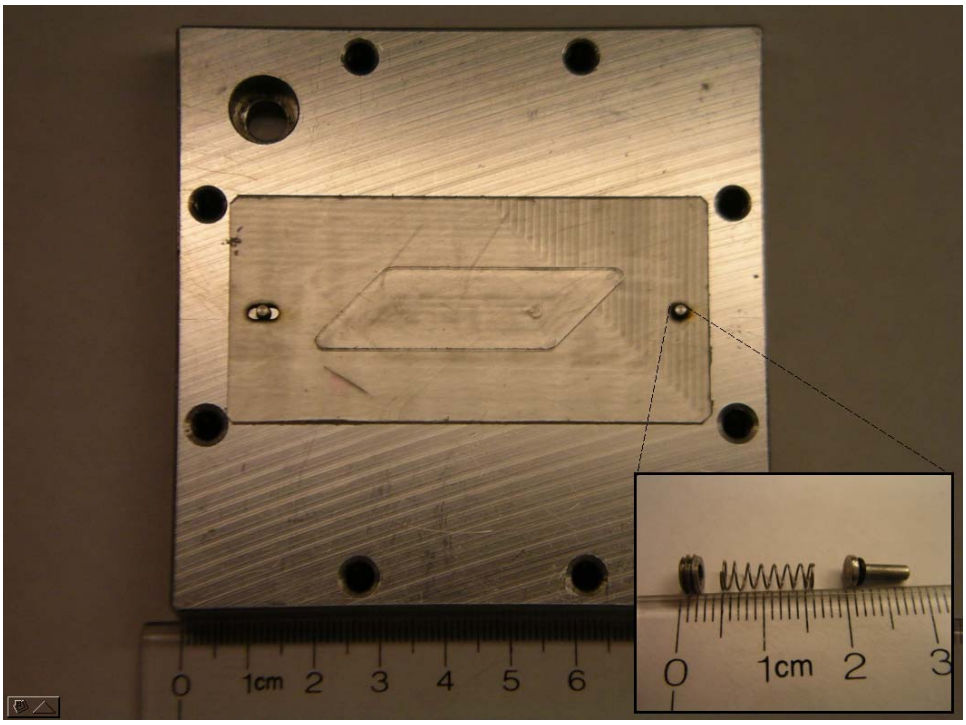

Figure 9: Registration fixture for MNM. Used to align the APET parts during Clearweld deposition and transmission laser welding. Inset picture shows a disassembled alignment pin. The pins are independently supported by compression springs that prevent damage to the quartz plate used for clamping.

2.8 Fluidic Control

Both the MTF and MNM were interfaced with the same fluidic control system (Fig. 10) [11]. For tests with the MTF in dead end flow, the path from the fixture to the retentate reservoir was removed and plugged. For tests in the MNM in cross flow, the path to the retentate reservoir was preserved and an adjustable bleed valve to atmosphere was used to control a pressure drop, thereby regulating fluid flow between the feed reservoir and retentate reservoir. Nitrogen gas supplied to the feed reservoir and retentate reservoir headspaces

provided the pressure to drive the system. The pressure was adjusted and monitored at the nitrogen cylinder tank regulator.

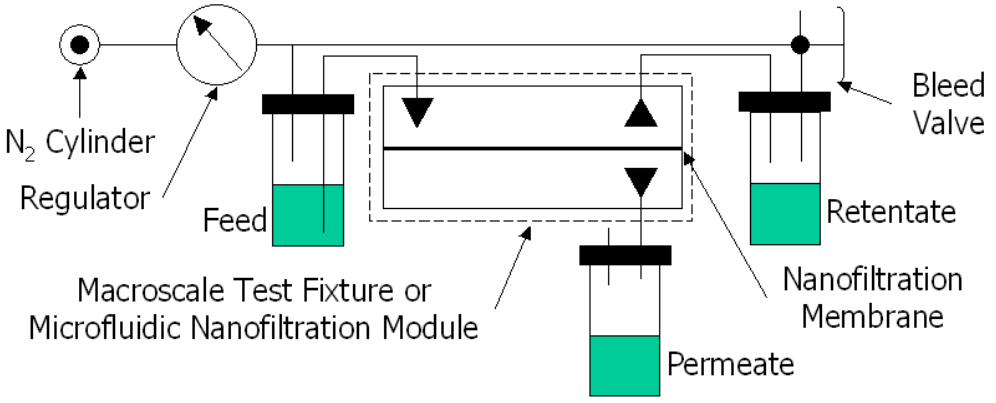

Figure 10: Fluidic control schematic for the MTF and the MNM. The pressure, supplied by the N_2 cylinder, drives both the transmembrane flux and the flow from the feed reservoir to the retentate reservoir. The bleed valve controls the pressure drop, and therefore the fluid flow, between the feed and retentate reservoir.

Three distinct types of glassware were used as reservoirs for the feed, permeate and retentate. For volumes of 10 mL or less, solvent rinse kits (Sigma-Aldrich, St. Louis, MO) were used as received. For volumes of 100 ml or less, a 100 mL pressure tube (Ace Glass, Vineland, NJ) was used with a PTFE adapter modified to accept the threaded head of the solvent rinse kit. For volumes 1000 mL or less, 1 L Wheaton bottles were used with a PTFE cap fabricated to accept ¼ in.-28 nuts and 1/16 in. O.D. PEEK tubing (Upchurch Scientific). Another piece of glassware, a Micromate 30 cc glass syringe (Popper & Sons, New Hyde Park, NJ) was used for manual flushing of fluidic channels when necessary.

Swagelok 1/16 in. stainless steel ball valves (Portland Valve & Fitting, Portland, OR) controlled the routing of N_2 gas. Luerlock fittings and 0.015 in. I.D. x 1/16 in. O.D. PEEK tubing (Upchurch Scientific, Oak Harbor, WA) were used for all other fluidic connections between components.

2.9 Data Collection

Masses of the permeate and retentate were found by the mass difference between the final and initial masses of the respective reservoirs. Volumetric flux was calculated as the product of mass flux and fluid density. For cross flow modes, retentate and permeate volumetric flow rates were held equal by adjustment of the bleed valve and monitoring of the drip rate into the reservoirs.

Fluorescence data was collected with a Luminescence Photometer (Perkin-Elmer, Waltham, MA) scanning from 350 to 700 nm with a fixed 25 nm offset between excitation and emission wavelengths and 5 nm excitation and emission slit widths using a quartz cuvette with a 1 cm path length. Absorbance data was collected with an Agilent 8453 UV-Visible Spectrophotometer (Agilent, Santa Clara, CA) from 190 to 1100 nm with 1 nm spectral resolution using a quartz cuvette with a 1 cm path length.

All errors are given as the standard deviation of a single set of at least three data points (and up to ten where possible) or as the average of the standard deviations of a collection of multiple sets. The fluorescence and absorbance data points used were recorded automatically by the given instrument as the average of three measurements at each wavelength. The standard deviations of the absorbance measurements were also calculated automatically and recorded but not used in this report.

3 Macromolecules in the MNM and MTF

3.1 Introduction

The goals of this research were to assess the performance of the membrane at lower-than-normal pressures, compare the MNM with the MTF to identify any potential compromise of the membrane during assembly of the MNM, determine a MWCO, and to develop fluid handling techniques with more stable, less expensive analytes. To address these goals, Rhodamine B (RhB, MW = 479) was used in the initial testing as a surrogate for G–0.5 (MW = 404) chosen for ease of detection, a similar molecular weight, high solubility in MeOH, low cost, and stability at standard conditions.

The reasons for using PAMAM dendrimers were twofold. Firstly, PAMAM dendrimers serve as a model macromolecule for an iterative synthetic process within a nanofactory in which the product of one reaction becomes the reagent for the next. Secondly, PAMAM dendrimers can be used to characterize the membrane since they are spherically symmetric, well analyzed in the literature, and commercially available with a high degree of monodispersity. However, this study was limited to the use of half-generation PAMAM dendrimers due to material compatibility issues discussed in Section 2.5.

3.2 Experimental Design and Results

Prior to initial use, each membrane was rinsed a minimum of 10 times for 20 min each at 1.4 bar in dead end flow until a stable flux was observed. This pre-conditioning is necessary to remove an impregnating oil that stabilizes the dry membrane during shipment and storage.

3.2.1 Rhodamine B (RhB)

Rhodamine B (RhB) was tested in the MTF and MNM at 10^{-7} M in 4 mM MA in MeOH. This relatively low feed concentration was chosen to eliminate the need for further dilution in order to facilitate detection. Rejections were determined from fluorescence data averaged over the range of 530-550 nm. Rejection of RhB at 1.4 bar was found to be .550 ± 0.005 for dead end flow in the MTF and 0.503 ± 0.007 for cross flow in the MNM (Figs. 11 and 12). Rejection vs. pressure data in the MTF shows a positive correlation from 1.4 to 6.9 bar obtained using dead end flow (Fig. 13).

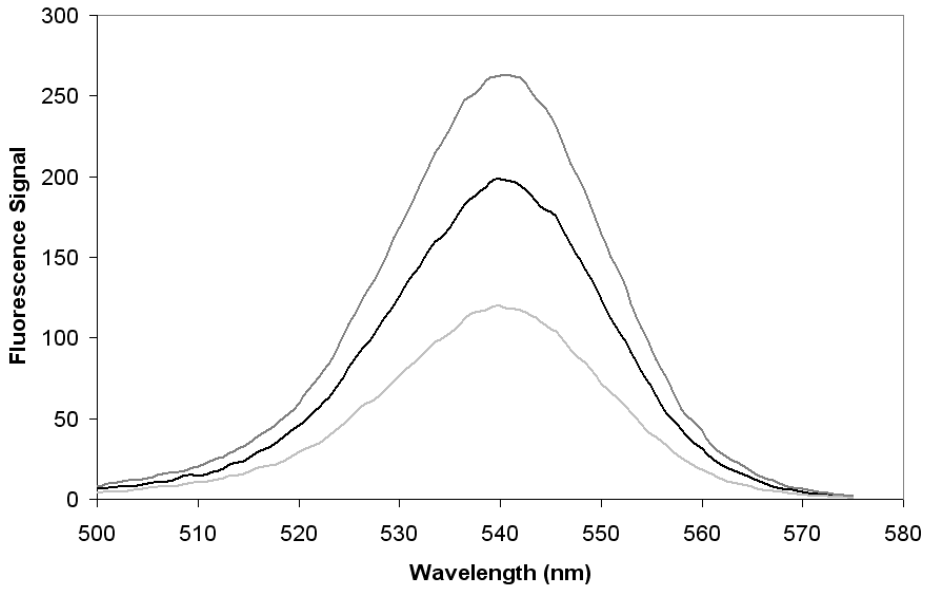

Figure 11: Fluorescence scan of 10^{-7} M RhB in MTF. Legend: black = feed; dark gray = retentate; light gray = permeate.

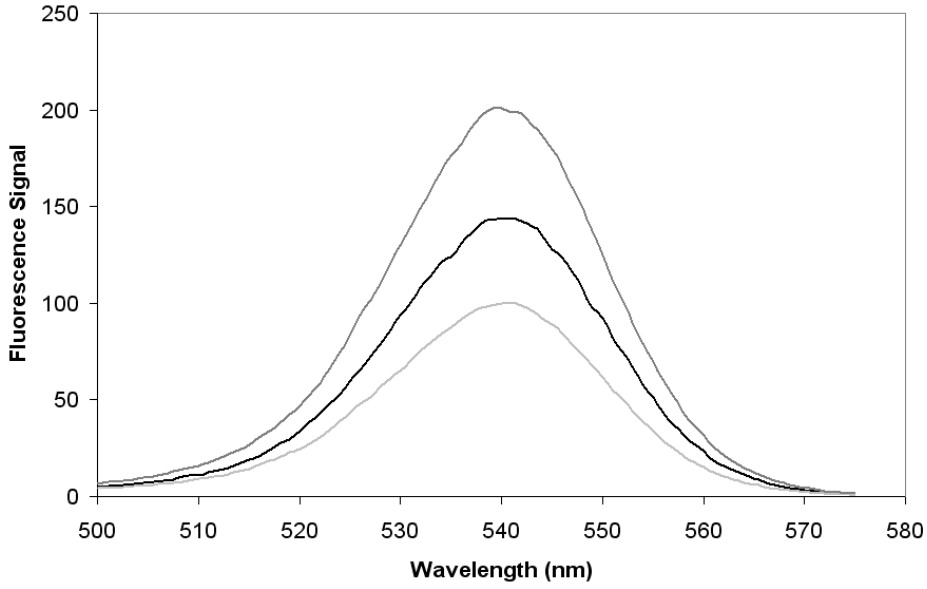

Figure 12: Fluorescence scan of 10^{-7} M RhB in MNM. Legend: black = feed; dark gray = retentate; light gray = permeate.

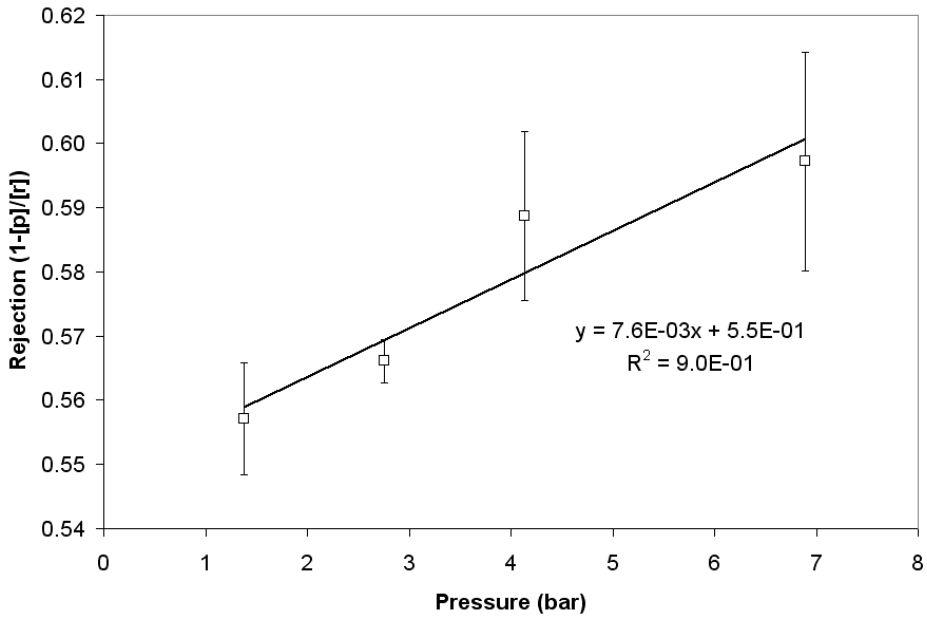

Figure 13: Rejection vs. transmembrane pressure in the MTF. Rejections of 10^{-7} M RhB in MeOH show a slightly positive correlation to pressure. Error bars are ± one standard deviation.

3.2.2 Half-Generation PAMAM Dendrimers

Half-generation PAMAM dendrimers were tested in the MNM at 1 g/L concentration in 4 mM MA in MeOH. These concentrations are approximately two orders of magnitude more dilute than values published for PAMAM synthesis [56] but represent the expected ratios of product and excess reagent following half-generation synthesis. These relatively low concentrations were chosen to limit the consumption of PAMAM and eliminate the need for further dilution in order to facilitate detection. Absorbance of half-generation PAMAM dendrimers was scanned against a blank of 4 mM MA. Rejections were determined from absorbance data averaged over the range of 225-235 nm

for G-0.5 and 230-240 nm for the higher generations. Figures of representative absorbance spectra and calculated rejections are shown in Appendix B.

The rejections of the half-generation PAMAM dendrimers follow a curve with a shape characteristic of nanofiltration membranes (Fig. 14). A MWCO = 2.3 kDa was calculated by extrapolating the linear fit of the uppermost three data points to a rejection of 0.90. The MWCO = 220 Da at 55 bar reported for the membrane is an order of magnitude lower than this MWCO = 2.3 kDa at 1.4 bar. This negative correlation of MWCO with transmembrane pressure is expected for diffusion-dominated mass transport.

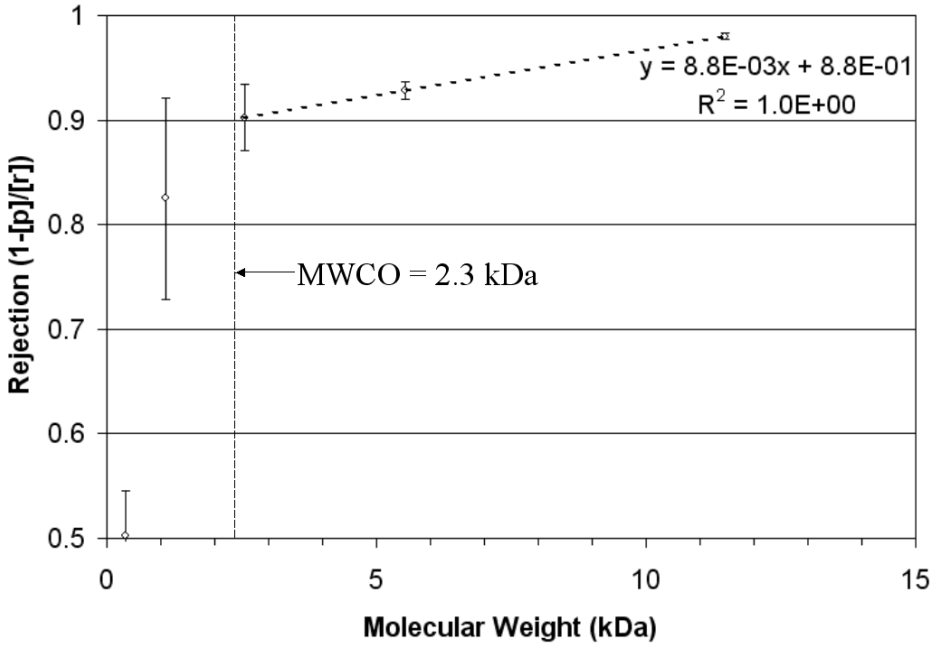

Figure 14: Molecular weight cutoff (MWCO) of half-generation PAMAM. Carboxyl-terminated half-generation PAMAM dendrimers were used to determine the MWCO in the MNM by extrapolating the linear fit of the uppermost data points to 0.90 rejection. Error bars are ± one standard deviation.

The permeance in the MNM was seen to be relatively stabile around 5 L m^{-2} h^{-1} bar^{-1} during the testing of half-generation PAMAM dendrimers (Fig. 15). This suggests that extended use of the membrane is possible with no fouling or degradation of the membrane or the module itself.

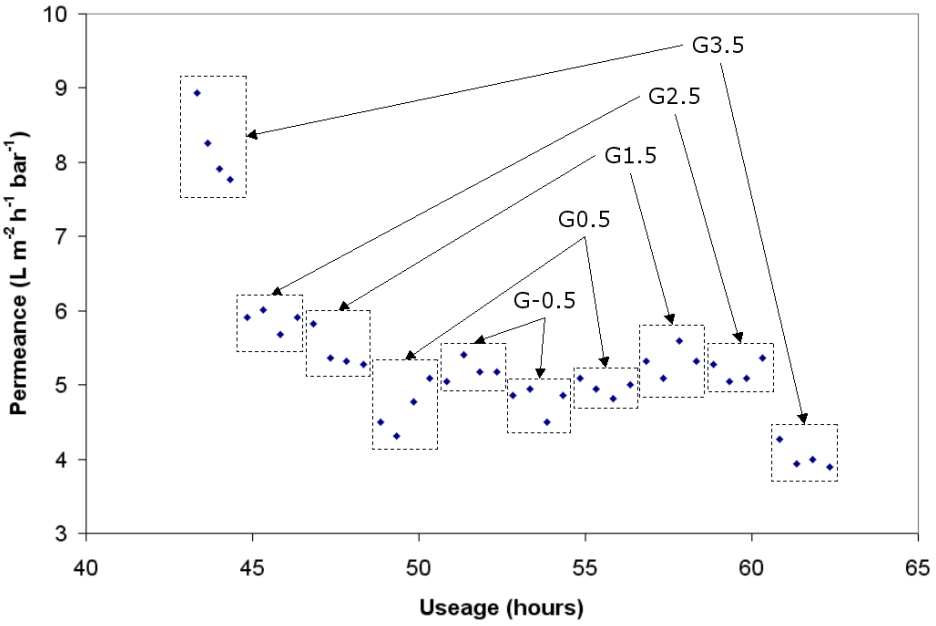

Figure 15: Permeance of the MNM during the purification of PAMAM half-generations.

3.3 Discussion

Performance of RhB in the MTF and MNM were found to be comparable indicating that the both devices can be used for nanofiltration purification at lower-than-normal transmembrane pressures. Purification of post-synthetic half-generation PAMAM dendrimers does not appear to be practical with the MNM at the given operating conditions due to relatively low rejections (<0.99)

that predict extensive loss of product from a post-synthetic stream. Further work is needed assess whether higher concentrations and higher pressures might result in rejections high enough to justify post-synthetic purification of half-generation PAMAM using the STARMEM 122 membrane.
Of greater concern is the incompatibility of the membrane with full-generation PAMAM.

Alternatively, ceramic membranes, with excellent chemical compatibility could be used in place of the polymer membrane [59-63]. However, ceramic membranes are typically limited to > 800 μm in thickness making them less attractive for microfluidic applications. The extremely high melting points of most ceramics eliminate the possibility of welding them to polymer substrates. Therefore, the fabrication strategy described here for the MNM may not prove viable for integration of ceramic nanofiltration membranes into a microfluidic format. The MTF design could easily incorporate commercially available ceramic membranes, commonly available in a thin disk form.

4 Diafiltration of Au_{11} in the MTF

4.1 Introduction

The goal of this study was to demonstrate that the desired Au_{11} product could be retained from a post-synthetic product stream while the anticipated major byproduct, triphenylphosphine (PPh_3), would pass into the permeate. The MWCO of 2.3 kDa determined in the preceding section suggests the practicality for purification of post-synthetic Au_{11} in which the targeted product has a mass > 4 kDa and the dominant byproduct has a mass < 0.3 kDa. Only the MTF was used in the remainder of this body of work because the supply of MNMs had been exhausted in prior testing, the contract to fabricate them could not be renewed and efforts to fabricate them in-house proved unsuccessful.

The details of this study are reported in chronological order since the same membrane was used in all trials and there is some evidence of carry-over or history of the membrane depending on the content of the previous feed.

4.2 Experimental Design

The concentration of Au_{11} was calculated with a calibration curve ($y = 5.2x$, $R^2 = 0.99$) from absorbance data of Au_{11} standards averaged over the range of

410-420 nm. This wavelength range was chosen because it encompasses a absorbance peak indicative of smaller gold nanoparticles such as Au_{11} [64] and also because none of the potentially interfering species absorb in this region with the exception of other possible gold nanoparticle species. A second absorbance peak indicative of smaller gold nanoparticles exists just above 300 nm. This peak was used to identify the presence of Au_{11} but was not used for quantification due to the presence of other species that absorb in that region.

Detection of PPh_3 was a bit more problematic due to strong absorbance in the UV by other known species in that region (EtOH, THF, Au_{11}) as well as unknown interferrents thought to be leaching out of system polymer elements. Techniques employed to address these issues are discussed below. A triad of absorbance peaks in the 250-280 nm region was also used to identify the presence of PPh_3 (Fig. 16). Calibration curves based on standard solutions were used for concentrations of 0.01 to 1 g/L ($y = 2.0x - 0.1$, $R^2 = 1.0$) at 305 nm and for concentrations of 0.001 to 0.1 g/L ($y = 12x$, $R^2 = 1.0$) at 266 nm.

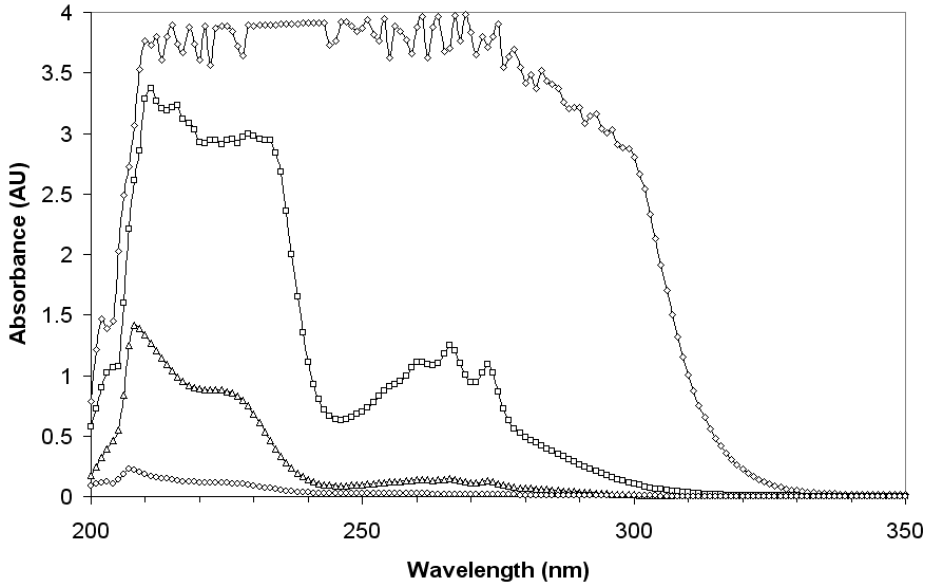

Figure 16: Absorbance spectra of the calibration standards for PPh_3. Legend: ◇ = 1.0 g/L; □ = 0.1 g/L; △ = 0.01 g/L; ○ = 0.001 g/L.

Throughout this study, a mixture of 50% v/v THF/EtOH was used as the solvent and will be referred to as 50% THF from this point forward. For all absorbance data a blank of neat EtOH was used. This was chosen because a single source of EtOH existed in large quantity assumed to be of consistent and uniform composition. Also, by using a pure solvent as the blank, changes in concentration of volatile mixtures due to evaporation were not a concern. In contrast, the composition of the 50% THF cannot be assumed to be consistent throughout the testing since it was prepared in 1 L quantities on an as-needed basis using low precision glassware. Also, changes in concentration due to evaporation could not be fully controlled although efforts were made to minimize such effects. In response to this uncertainty, UV-vis absorbance

spectra of the relevant 50% THF was taken along with the set of analytical samples for that day.

A fresh membrane was cut to size, placed in the MTF and preconditioned with 50% THF for 43 h at 2.8 bar prior to use to fully flush out all the impregnating oils.

Throughout the testing, small absorbance signals were seen in the UV spectra (200-300 nm) of permeate and retentate samples obtained from 50% THF. The UV absorbance spectra immediately following preconditioning are indicative of the observed magnitudes and relative shapes (Figs. 17 and 18).

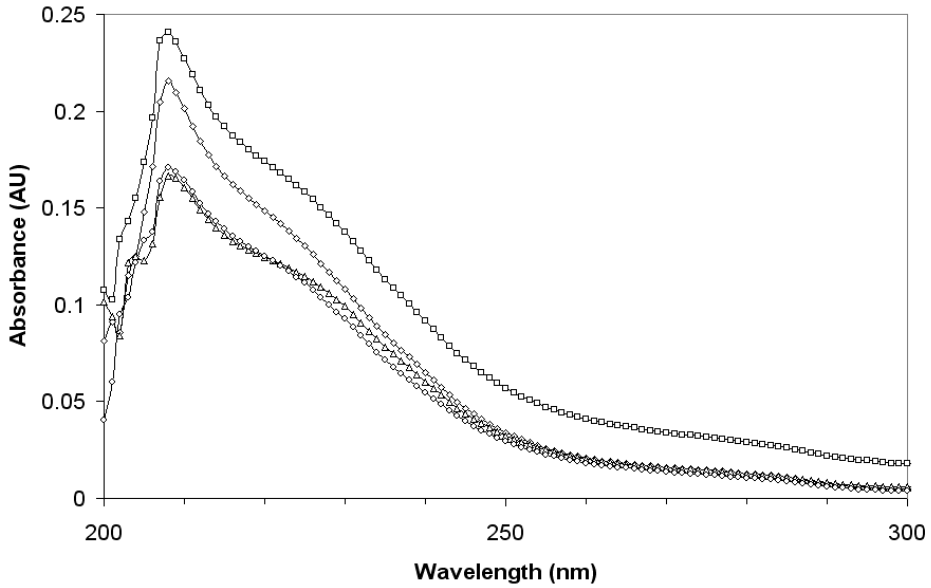

Figure 17: Retentates immediately following the preconditioning of the MTF. Legend: sequence of runs = □, ◇, △, ○.

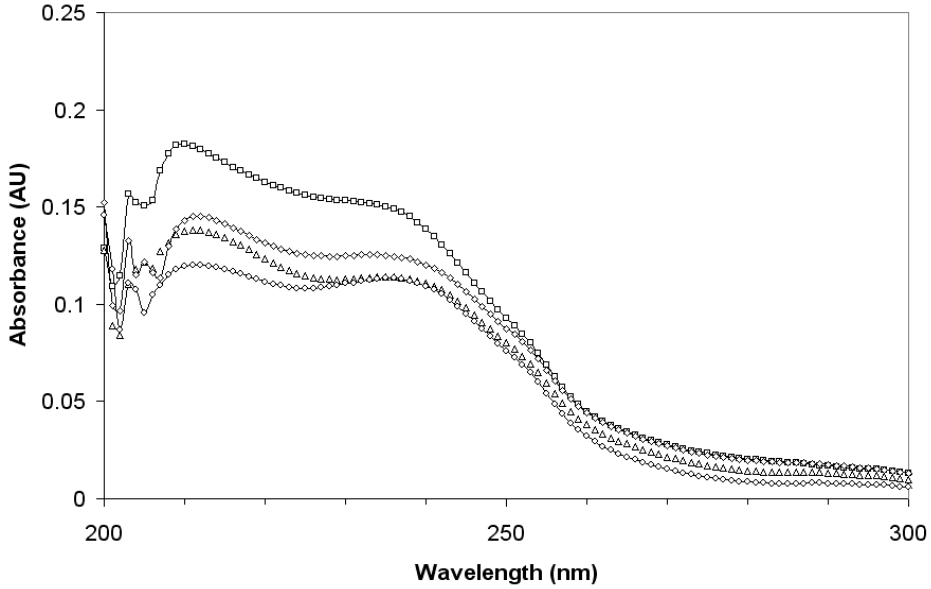

Figure 18: Permeates immediately following preconditioning in the MTF. Legend: sequence of runs = □, ◇, △, ○.

The origin and identity of the interferrent species are unknown but it is thought to arise from leaching out of one or several of the polymer components that comprise the system. Fortunately, the absorbance due to the unidentified interferrent is limited to the UV region and is relatively small in magnitude. It does not contribute to the signal at 410-420 nm used for Au_{11} detection. However, the interferrent absorbance does overlap the 250-280 region used for PPh_3 detection and would contribute significantly to a signal from a low PPh_3 concentration on the order of 0.01 g/L.

Because of this, at least one permeate and retentate sample was collected prior to each set of runs using a feed of 50% THF. The UV-vis absorbance spectra

of those samples were then manually subtracted from the respective permeate and retentate spectra of the analytical samples for that day. For samples that were diluted to improve detection, the absorbance spectrum of the 50% THF was used instead for manual background subtraction on the assumption that the interferrent signal had been diminished via dilution to the point of being negligible.

Whenever the feed was changed, efforts were made to prevent carry over of one set of analytes to the next. These efforts, stated in chronological sequence, included: (1) rinsing all reservoirs, tubing and connectors a minimum of 3x with EtOH (6x in the post-synthetic Au_{11} trials) and once with 50% THF; (2) rinsing the upper channel at least three times with 50% THF (filling, allowing all plugs to leak under pressure, and draining completely); (3) running the system for at least one hour at 1.4 bar with 50% THF to flush the membrane and to flush the sintered frit of the lower channel; (4) running the system for at least another 20 min at 1.4 bar with 50% THF; and (5) collecting the permeate and retentate of the final run for UV-vis absorbance analysis to identify any residual contaminants.

4.3 Results

4.3.1 Au_{11} and PPh_3 Standards

To evaluate the performance of Au_{11} and PPh_3 in the MTF, standards of both were prepared from crystalline stock by massing the solid and dissolving with 50% THF in volumetric glassware. The mixtures were sonicated for 15 min to promote dissolution. Relatively low concentrations of Au_{11} were used so that further dilution would not be necessary for detection and to minimize the consumption of the limited quantity of Au_{11} stock.

4.3.1.1 Trial 1: Au_{11} Standards

Trial 1 was conducted with $[Au_{11}]_f = 0.04$ g/L, P = 1.4 bar, $V_f = 5$ mL, $V_r = 2.5$ mL, with samples of the permeate and retentate collected every 20 min. A total of four retentates and four permeates were collected. The absorbance spectra of the retentates showed a high degree of consistency between runs with an average signal of 0.37 ± 0.01 AU in the 410-420 nm range. This is to be expected since the product stream channel was emptied prior to each run, including the first run, and each retentate began with the same feed. The absorbance spectra of the permeates showed a low degree of consistency between runs with an average signal of 0.3 ± 0.15 AU in the 225-235 nm range. This is also to be expected since the permeate channel could not be emptied prior to each run including the first in which it was full of 50% THF.

For these reasons the spectra of the last permeate and last retentate of any given set of runs were used for all analyses from this point forward.

The spectrum of the final retenate has the same overall shape and higher signal strength as compared to the feed indicating an increase in the concentration of Au_{11}, as expected (Fig.19). The absorbance spectrum of the final permeate shares a similar shape with an overall lower signal strength indicating that some, but very little, of the Au_{11} was transported across the membrane. A rejection of 0.964 ± 0.001 was calculated in the 410-420 nm range.

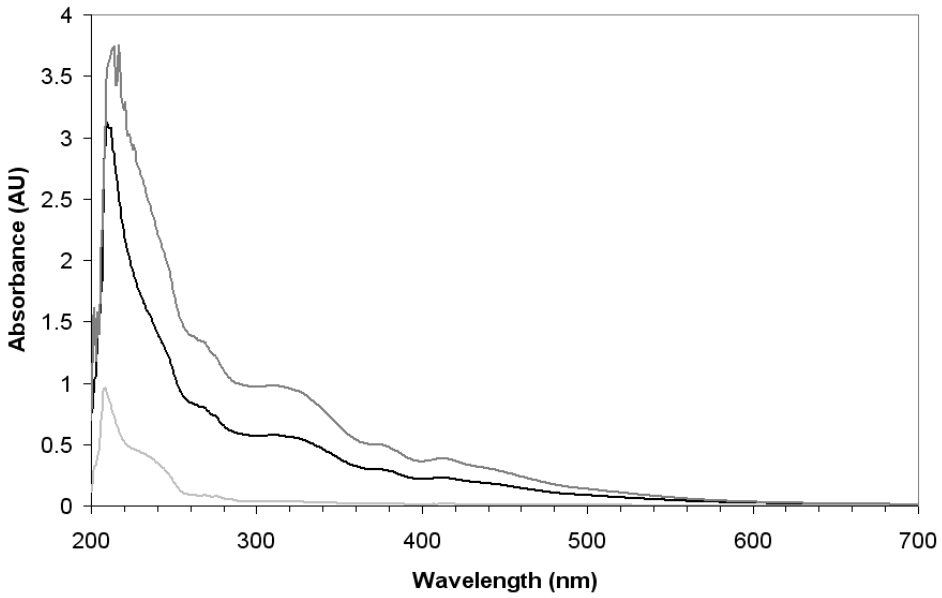

Figure 19: Trial 1 filtration of Au_{11} standard at 0.04 g/L. Legend: black = feed; dark gray = retentate; light gray = permeate.

4.3.1.2 Trial 2: PPh_3 Standard

Trial 2 was conducted with $[PPh_3]_f = 0.1$ g/L, P = 1.4 bar, $V_f = 5$ mL, $V_r = 2.5$ mL with samples of the permeate and retentate collected every 20 min. A rejection average of 0.375 ± 0.008 was calculated from the absorbance signals from 265-275 nm of the final permeate and retentate collected (Fig. 20). This agrees well with an extrapolation of the MWCO data collected with the half-generation PAMAM dendrimers. It also indicates that PPh_3 can be removed from a post-synthetic Au_{11} product stream via a diafiltration method using this nanofiltration membrane.

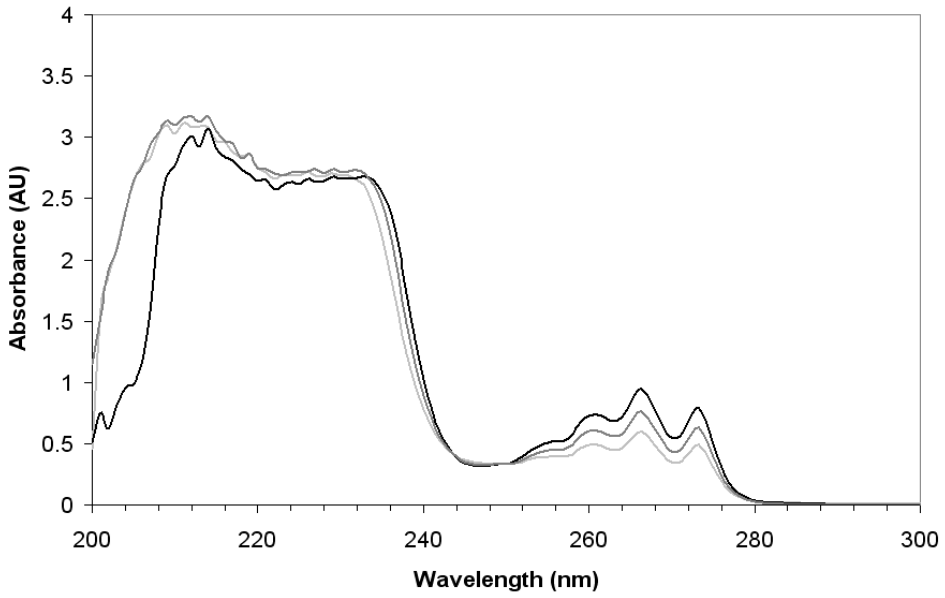

Figure 20: Trial 2 filtration of PPh_3 standard at 0.1 g/L. Legend: black = retentate; dark gray = feed; light gray = permeate.

4.3.1.3 Trial 3: Au_{11} Standards

Trial 3 was conducted with the combined retenates of Trial 1 $[Au_{11}]_f = 0.07$ g/L (calculated from the calibration curve), P = 1.4 bar, $V_f = 5$ mL, $V_r = 2.5$

mL. Only one permeate and one retentate sample were collected. As before, the shape and magnitude of the feed and retentate spectra indicate that Au_{11} was retained and concentrated (Fig. 21). A rejection of 0.998 ± 0.001 was calculated in the 410-420 nm range. However, the rejection is likely skewed positive by the fact that all of the permeate was collected in one sample which included the 50% THF that filled the permeate channel prior to the runs and excluded the permeate that remained in the channel at the conclusion of the runs.

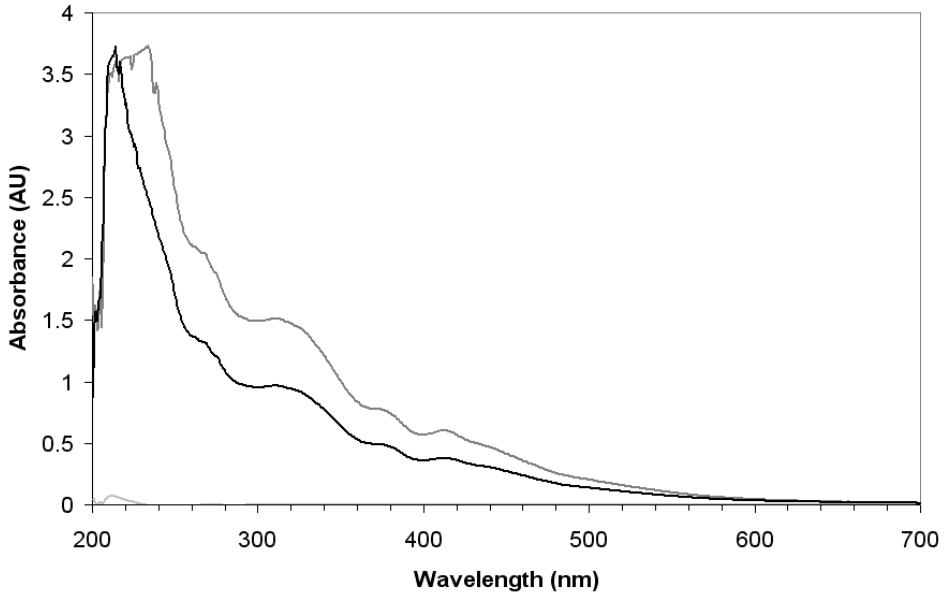

Figure 21: Trial 3 filtration of retentates of the Au_{11} standard at 0.04 g/L. Legend: black = feed; dark gray = retentate; light gray = permeate.

The absorbance spectrum of the permeate of Trial 3 shows a very low signal below 300 nm in sharp contrast to that of the permeate of Trial 1 (Fig.19). This might be interpreted that the Au_{11} standard, purified by conventional means, can actually be further purified by this filtration method with the

impurities passed to the permeate in Trial 1. However, the difficulty in accurately sampling the permeate produced by the MTF (described above in 4.3.1.1) could have resulted in a simple dilution of the permeate producing misleading results. Further testing is needed to fully assess this possibility.

4.3.1.4 Trial 4: Au_{11} Standards

Trial 4 was conducted with $[Au_{11}]_f = 0.1$ g/L (as prepared from the standard), P = 1.4 bar, V_f = 25 mL, V_r = 2.5 mL. In this trial the permeate was collected every 20 min but the retentate was only collected after the final run. The retentate was concentrated six-fold (5.86 ± 0.02) as averaged from 450-460 nm along with a rejection of 0.992 ± 0.001 in the same spectral region (Fig. 22). This demonstrates that concentration of Au_{11} is possible with high rejection.

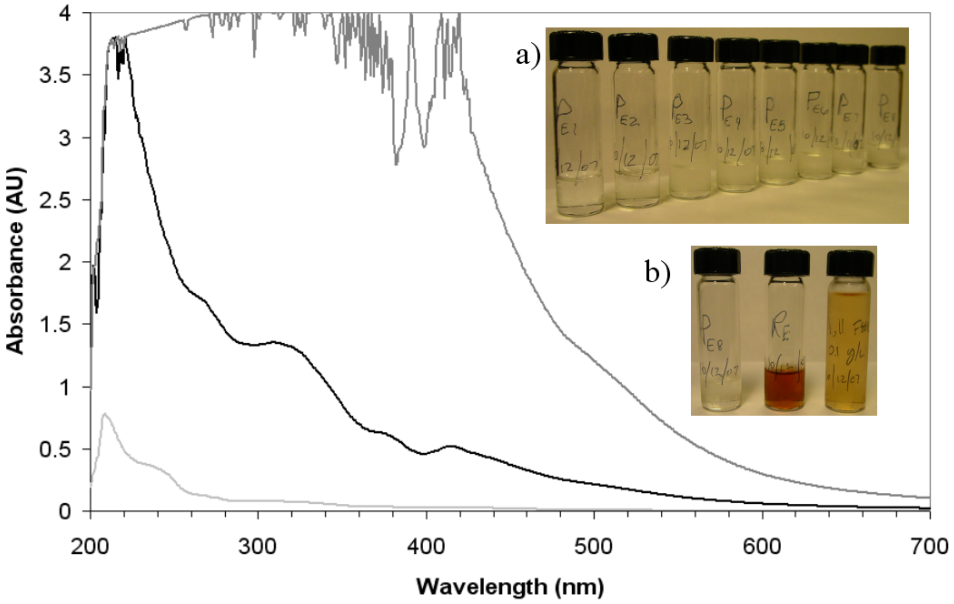

Figure 22: Trial 4 filtration of Au_{11} standard at 0.1 g/L. Legend: black = feed; dark gray = retentate; light gray = permeate. Feed volume = 30 mL, retentate volume = 2.5 mL. Inset photos are: a) all permeates; b) last permeate, retentate and feed from left to right.

4.3.1.5 Trial 5: Diafiltration of PPh_3

To further evaluate the performance of PPh_3 in the MTF, a series of four steps was conducted to demonstrate that the concentration of PPh_3 could be reduced via diafiltration with successive filtrations and dilutions. A solution of 1.0 g/L PPh_3 in 50% THF, prepared from the solid, was the feed for the first step as an approximation of the 1.4 g/L PPh_3 concentration expected in a post-synthetic feed. Trial 5 was conducted with P = 1.4 bar, V_f = 25 mL, and V_r = 2.5 mL. Samples were refrigerated whenever possible to minimize possible oxidation of PPh_3. The absorbance spectra of the four PPh_3 diafiltration retentates indicate that PPh_3 can be removed from a 50% THF solution by this method (Fig. 23).

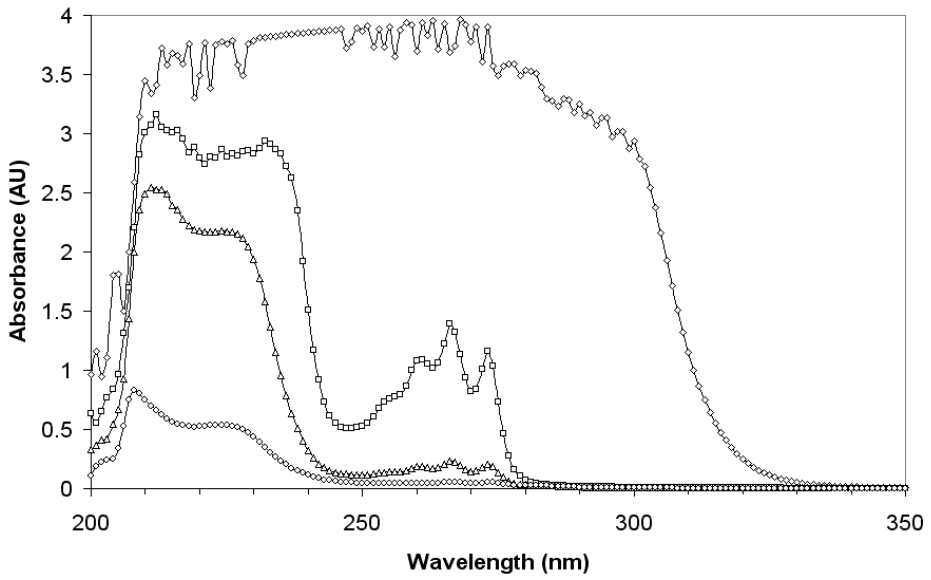

Figure 23: Trial 5 retentate absorbance spectra in the diafiltration of PPh_3 in the MTF. Conditions: P = 1.4 bar, V_f = 25 mL, V_r = 2.5 mL. Legend: ◇ = Step 1; □ = Step 2; △ = Step 3; ○ = Step 4.

Greater detail of the performance can be seen in a plot of the rejection and retentate concentration over the series of steps (Fig. 24). The decreases in concentration agree well with the performance predicted using Equation 3 and shown in Figure 2 (Section 1.2) assuming the rejection of ~40% found for 0.1 g/L PPh_3 (Section 4.3.1.2). However, the theoretical treatment in Section 1.2 provides information about the *molar ratio* of the original feed and the final retentate. In contrast, the empirical treatment shown here provides information about the *concentration* of the retentate. In order to bring the two treatments in line, the retentates in Figure 24 must be mentally diluted by a factor of ten to the original V_f. Once this is applied, the concentration of PPh_3 is seen to decrease between three and four orders of magnitude over four filtration steps.

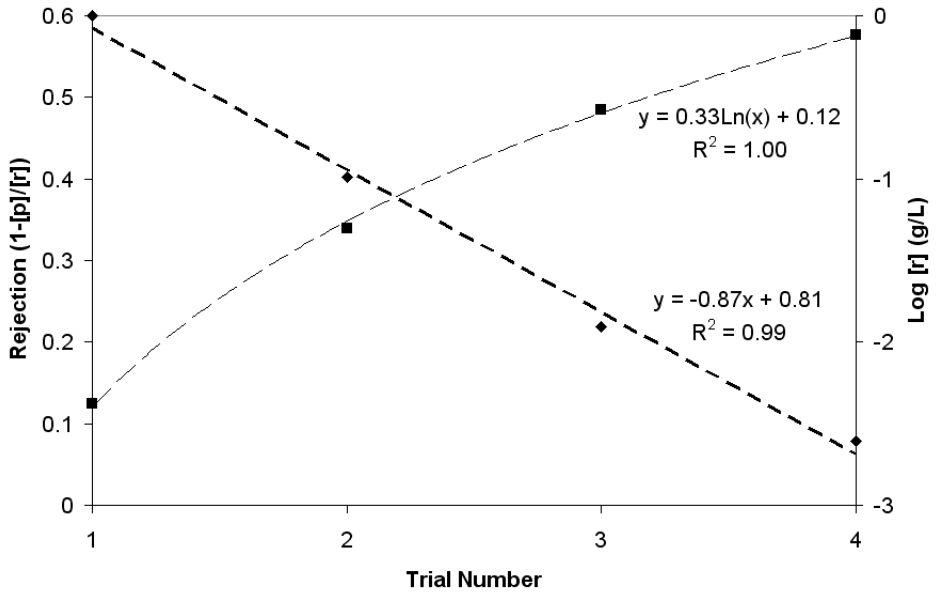

Figure 24: Trial 5 rejections and concentrations in the diafiltration of PPh_3 in the MTF. Conditions: P = 1.4 bar, V_f = 25 mL, V_r = 2.5 mL. Legend: ■= Rejection of PPh_3; ◆= Concentration of PPh_3 in the retentate. Concentrations are calculated using a calibration curve developed from standard solutions at 266 nm and 305 nm.

There is yet another twist to all of this. The theoretical treatment assumes a constant rejection, independent of concentration. In Figure 24 we see that the rejection ranges from 0.12 to 0.58 as the concentration decreases. This is in good agreement with theory since diffusive transport across the membrane is dependent upon a concentration gradient. A decrease in the concentration gradient would decrease diffusive transport thereby decreasing the relative concentration in the permeate and increasing the calculated rejection. Regardless of these subtleties, everything indicates that PPh_3 will pass through the membrane and be removed from post-synthetic Au_{11} product stream in significant quantities via diafiltration.

4.3.2 Purification of Post-Synthetic Au_{11}

In the preceding sections it was demonstrated that Au_{11} is retained during filtration in the MTF at rejections < 0.99 and that PPh_3 moves across the membrane during filtration at rejections ranging from roughly 0.12 to 0.60. These findings suggest the feasibility of purification of post-synthetic Au_{11} via diafiltration.

All post-synthetic Au_{11} samples were prepared from reagents at 40 mM concentrations in the 1:1 stoichiometric ratio given in Equation 4. Assuming the reaction goes to completion, post-synthetic concentrations of $[Au_{11}(PPh_3)_8Cl_3]$ = 8.0 g/L and $[PPh_3]$ = 1.4 g/L in 50% THF should exist in post-synthetic samples. All samples were refrigerated or kept on ice whenever possible to minimize Au_{11} degradation and PPh_3 oxidation.

4.3.2.1 Trial 6: Post-Synthetic Au_{11}

A series of four diafiltration steps were taken to purify a post-synthetic sample of Au_{11}. The sample was used as received. The initial V_f = 10 mL was not diluted in the first step. However, in subsequent steps the retentate from the prior step was diluted with 50% THF to form V_f = 25 mL. All other parameters were held constant throughout: P = 1.4 bar, V_r = 2.5 mL. Each step lasted a full day including absorbance measurements. The full trial spanned

five days separated by overnight stays in the refrigerator and one full day of no activity between the third and fourth step.

The absorbance spectra of the feed, retentate and last permeate, each diluted by 100x with 50% THF, along with the calculated rejection for each of the four steps are shown in Figures 25-28. A photo is inserted for each step showing the undiluted feed, permeates and retentate. Note that the Step 2 permeates decrease in color as the runs progress indicating an increase in Au_{11} rejection: a decreasing permeate concentration concurrent with an increasing retentate concentration.

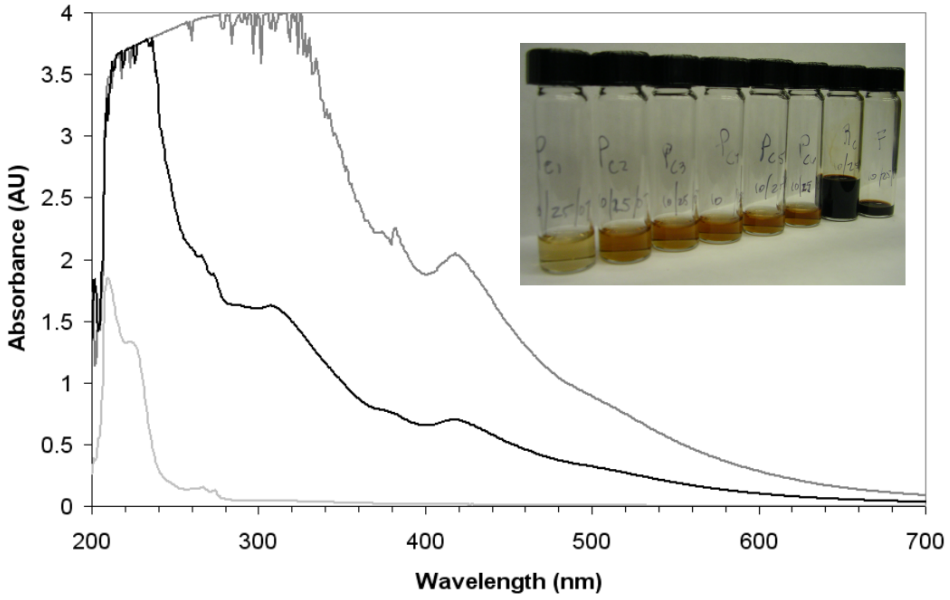

Figure 25: Diafiltration of post-synthetic Au_{11}, Trial 6, Step 1. Legend: black = feed; dark gray = retentate; light gray = permeate. All samples were diluted by 100x to allow absorbance measurements. Rejection = 0.991 averaged over 410-420 nm. Photo insert: undiluted permeates, retentate and feed.

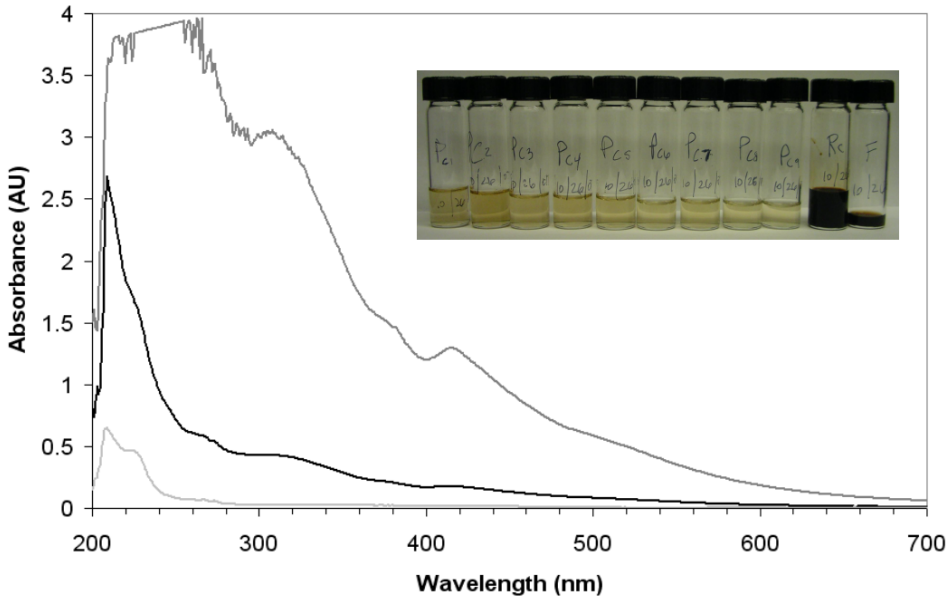

Figure 26: Diafiltration of post-synthetic Au_{11}, Trial 6, Step 2. Legend: black = feed; dark gray = retentate; light gray = permeate. All samples were diluted by 100x to allow absorbance measurements. Rejection = 0.986 averaged over 410-420 nm. Photo insert: undiluted permeates, retentate and feed.

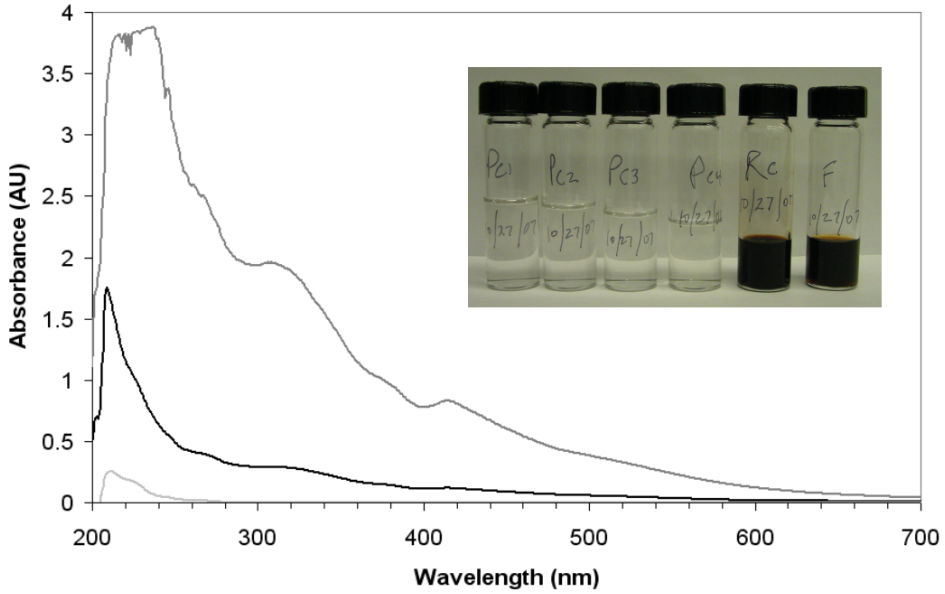

Figure 27: Diafiltration of post-synthetic Au_{11}, Trial 6, Step 3. Legend: black = feed; dark gray = retentate; light gray = permeate. All samples were diluted by 100x to allow absorbance measurements. Rejection = 0.996 averaged over 410-420 nm. Photo insert: undiluted permeates, retentate and feed.

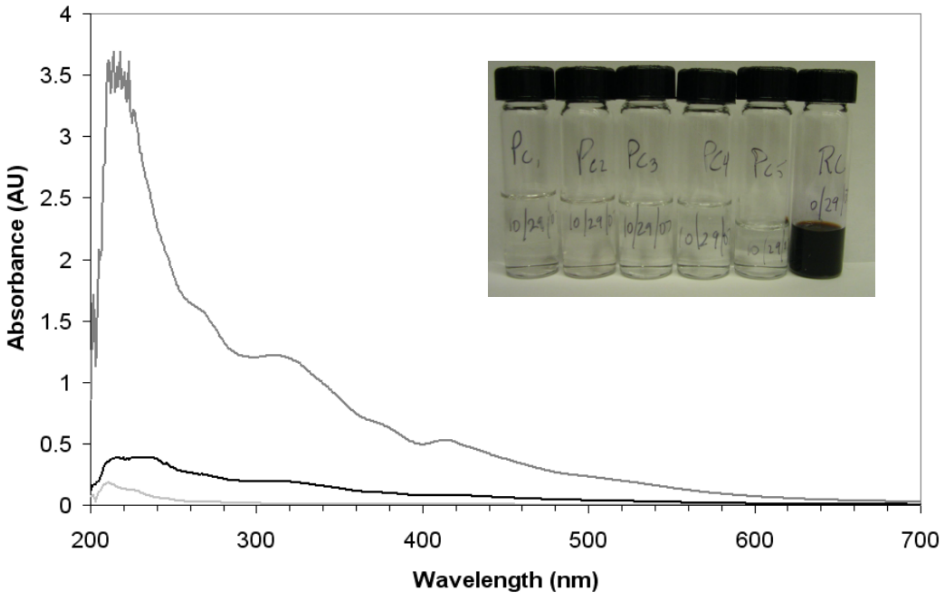

Figure 28: Diafiltration of post-synthetic Au_{11}, Trial 6, Step 4. Legend: black = feed (approximated from Step 3 retentate signal); dark gray = retentate; light gray = permeate. All samples were diluted by 100x to allow absorbance measurements. Rejection = 0.986 averaged over 410-420 nm. Photo insert: undiluted permeates and retentate.

The PPh_3 concentration decreases with each subsequent step (Figs. 29 and 30). A summary of Trial 6 is given in Figure 31 showing the final retentate, along with the original feed and the 0.1 g/L Au_{11} standard for comparison. The post-synthetic feed spectrum is comparable in shape and magnitude to that of the standard indicating the presence of Au_{11} at a concentration higher than 10 g/L and therefore greater than the anticipated 8 g/L. The PPh_3 triad is seen in the feed as well at the expected concentration of ~1 g/L. The final retentate also shows the strong presence of Au_{11} with a spectral shape similar to that of the feed and the standard. The retentate has a PPh_3 concentration comparable to that of the standard as seen in the magnification of the 255-280 nm spectrum. Together this demonstrates that Au_{11} was retained in the product stream to a significant extent and PPh_3 was removed from the product stream to a point comparable to conventional filtration.

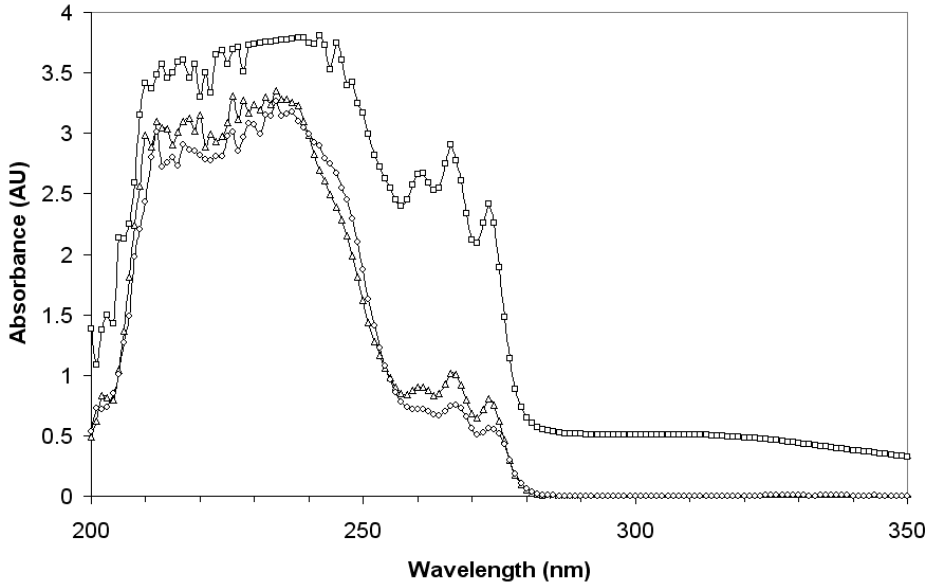

Figure 29: Permeates of the Trial 6 diafiltration of post-synthetic Au_{11}. Legend: □ = Step 2; △ = Step 3; ○ = Step 4 (data for Step 1 was inadvertently not collected). All permeates are shown at original, undiluted concentration. This shows a decrease in the concentration of PPh_3 for each step.

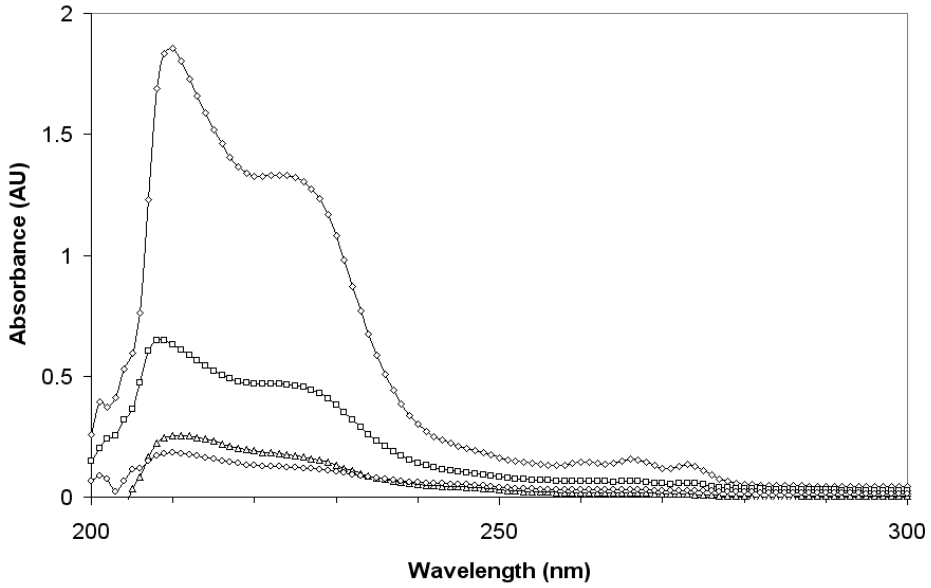

Figure 30: Diluted permeates of the Trial 6 diafiltration of post-synthetic Au_{11}. Legend: ◇ = Step 1; □ = Step 2; △ = Step 3; ○ = Step 4. All permeates are diluted with 50% THF by 100x. This shows a decrease in the concentration of PPh_3 for each step.

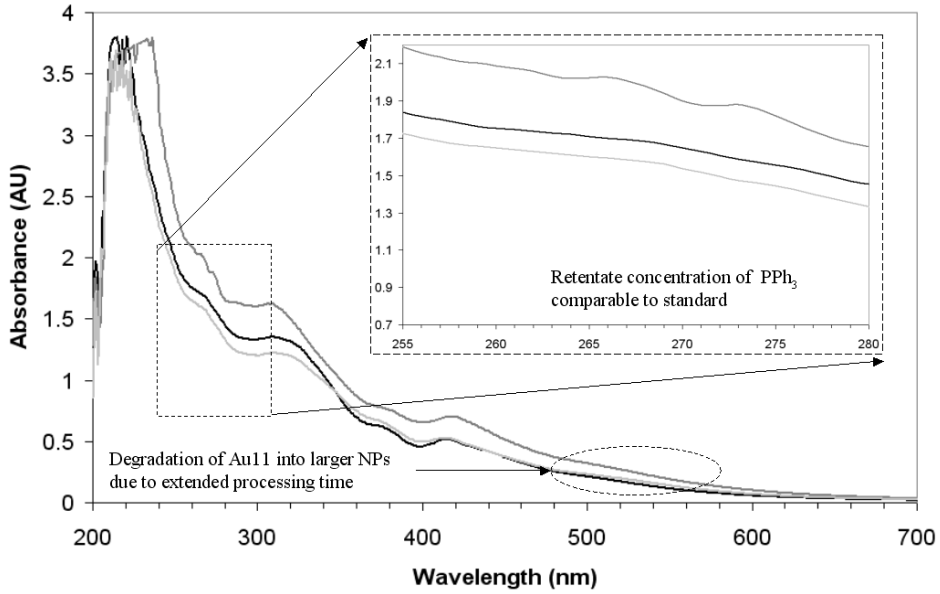

Figure 31: Diafiltration of post-synthetic Au_{11}Trial 6 Summary. Legend: black = Au_{11} standard, 0.1 g/L; dark gray = post-synthetic Au_{11}, 100x dilution; light gray = retentate after four diafiltration steps, 100x dilution.

The loss of Au_{11} is even more drastic than it appears by comparison of the magnitude of the absorbance considering that the $V_f \sim 10$ mL and $V_r \sim 2.5$ mL. This means that identical absorbance spectra would indicate a 75% loss of Au_{11} product. Analysis in the 410-420 nm range gives a feed concentration of 13.4 g/L and retentate concentration of 10.1 g/L indicating that only 19% of the product remains after purification. In other words, 81% of the product was lost due to processing.

A significant fraction of the loss is attributable to fluid handling such as rinsing and sampling. Samples of 100 μL were taken of the feed and retentate of each step in order to prepare a 100x dilution for UV-vis absorbance analysis. This

represents molar losses of 1% from the original post-synthetic sample, 0.4% from the other two feeds and 4% from the three retentates that were diluted to form the next feed. Losses, due to rinsing between steps, include conservative estimates of 100 μL remaining in the feed reservoir (1% or 0.4% as described above) and 100 μL remaining in the upper channel of the MTF (4%) at the end of each step. Over the course of the trial these sampling and handling losses account for ~30% loss of product. Fortunately, these losses could be avoided in the future with a continuous-flow system with on-chip detection for in situ analyses.

Another source of product loss is attributable to transport across the membrane to the permeate as described by the rejection. Assuming a constant rejection of 0.99, four steps at $V_f/V_r = 10$ would result in ~30% product loss. This can only be improved by increasing the rejection of Au_{11}.

The final source of product loss is due to plating out of gold as evidenced by photos of the vials used for overnight refrigerated storage of the retentates in the trial (Fig. 32). The vials show increasing levels of plating out over the course of the trial. Other plating out was seen to a lesser extent on the 10 mL feed reservoir. Fortunately, this is a time-dependent phenomenon that could be remedied with faster processing times. Assuming the other loss estimates are accurate, the remaining ~20% can be attributed to plating out.

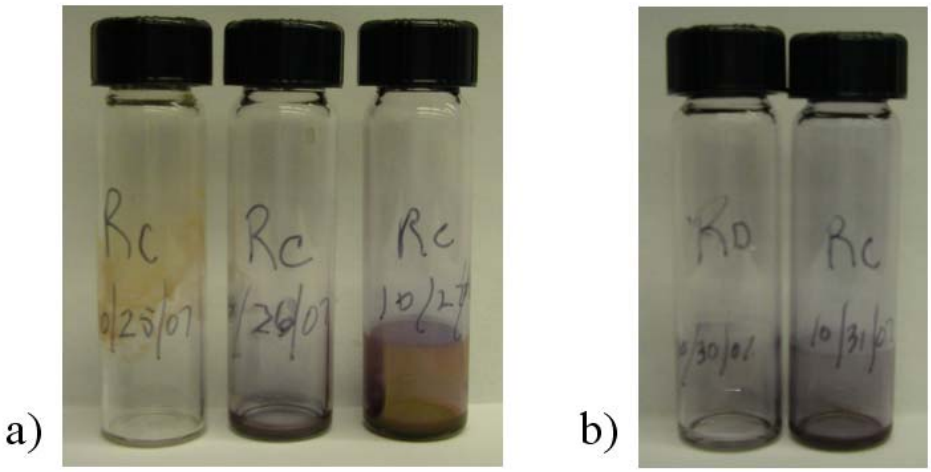

Figure 32: Photographic evidence of gold plating out onto the retentate vials. The vials from Trial 6 (a) show more plating out than those of Trial 7 (b). Both show a time dependency since the plating is more pronounced as the post-synthetic sample ages.

Of additional concern is the decrease in absorbance in the low 300 nm range and the coinciding increase in absorbance in the low 500 nm range suggesting that larger gold nanoparticles formed from the targeted Au_{11} over the course of the trial. These particles are assumed to absorb in the 410-420 nm range to the same extent as Au_{11} and therefore represent no net change in signal in that range.

4.3.2.2 Trial 7: Post-Synthetic Au_{11}

Conditions identical to those of Trial 6 (Section 4.3.3.1) were used in Trial 7 in order to assess the reproducibility of the results. However, an effort was made to decrease the overall process time to address the time-dependent factors discussed in the previous section. Steps 1 and 2 took one day each whereas

Steps 3 and 4 were done on the same day. The total process lasted three full days with two overnight stays under refrigeration.

The absorbance spectra of the feed, retentate and last permeate, each diluted by 100x with 50% THF, along with the calculated rejection for each of the four steps in are shown in Figures 33-36. A photo is inserted for each step showing the undiluted feed, permeates and retentate. Note that an increase in performance is seen in Step 2 as was similarly observed in Trial 6.

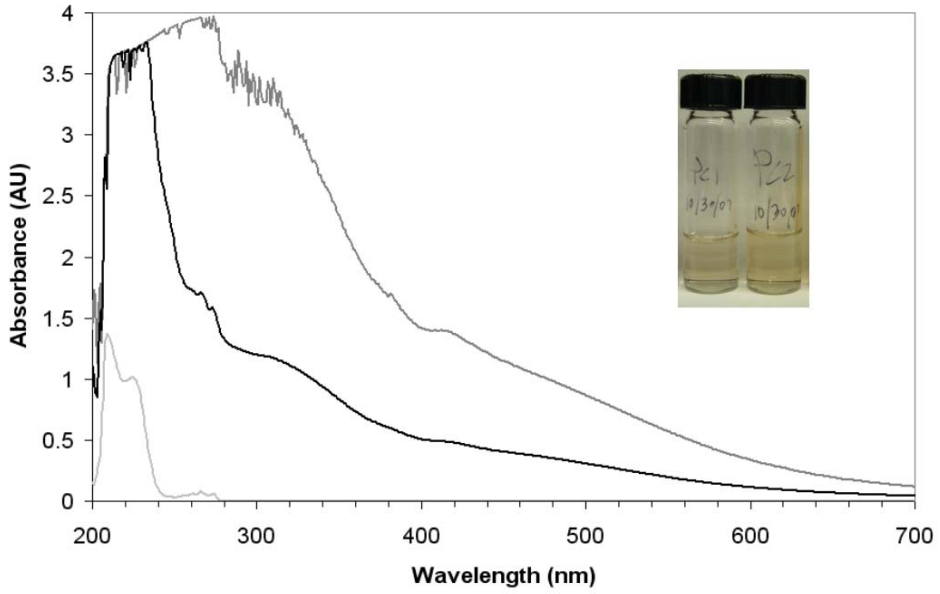

Figure 33: Diafiltration of post-synthetic Au_{11}, Trial 7, Step 1. Legend: black = feed; dark gray = retentate; light gray = permeate. All samples were diluted by 100x to allow absorbance measurements. Rejection > 0.999 averaged over 410-420 nm. Photo insert: undiluted permeates.

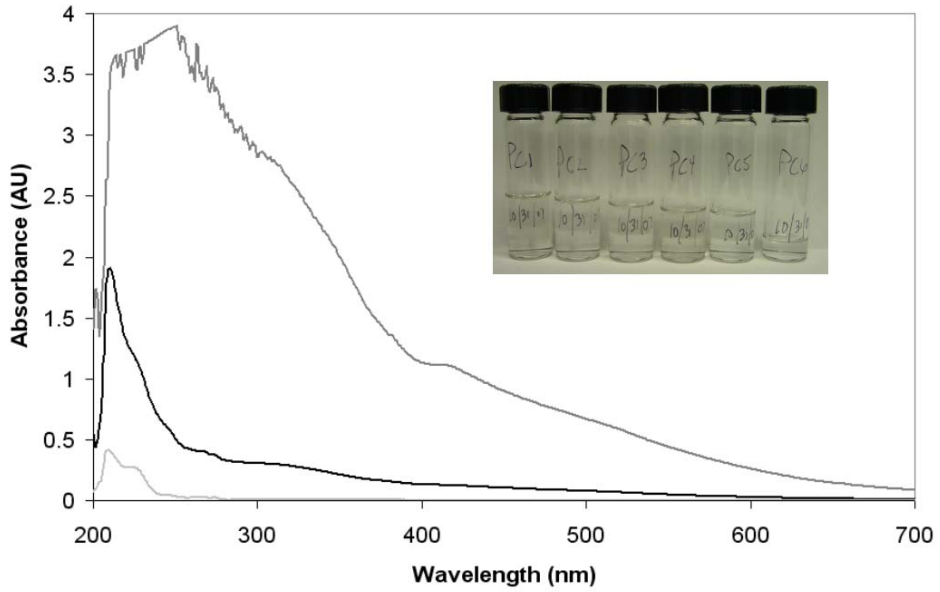

Figure 34: Diafiltration of post-synthetic Au_{11}, Trial 7, Step 2. Conditions: P = 1.4 bar, V_f = 25 mL, V_r = 2.5 mL. Legend: black = feed; dark gray = retentate; light gray = permeate. All samples were diluted by 100x to allow absorbance measurements. Rejection > 0.999 averaged over 410-420 nm. Photo insert: undiluted permeates.

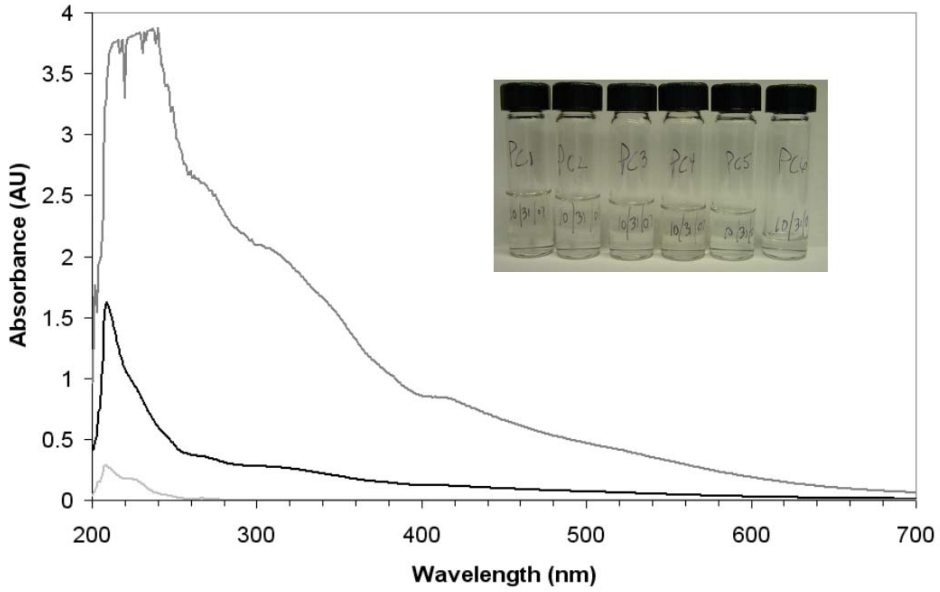

Figure 35: Diafiltration of post-synthetic Au_{11}, Trial 7, Step 3. Conditions: P = 1.4 bar, V_f = 25 mL, V_r = 2.5 mL. Legend: black = feed; dark gray = retentate; light gray = permeate. All samples were diluted by 100x to allow absorbance measurements. Rejection = 0.997 averaged over 410-420 nm. Photo insert: undiluted permeates.

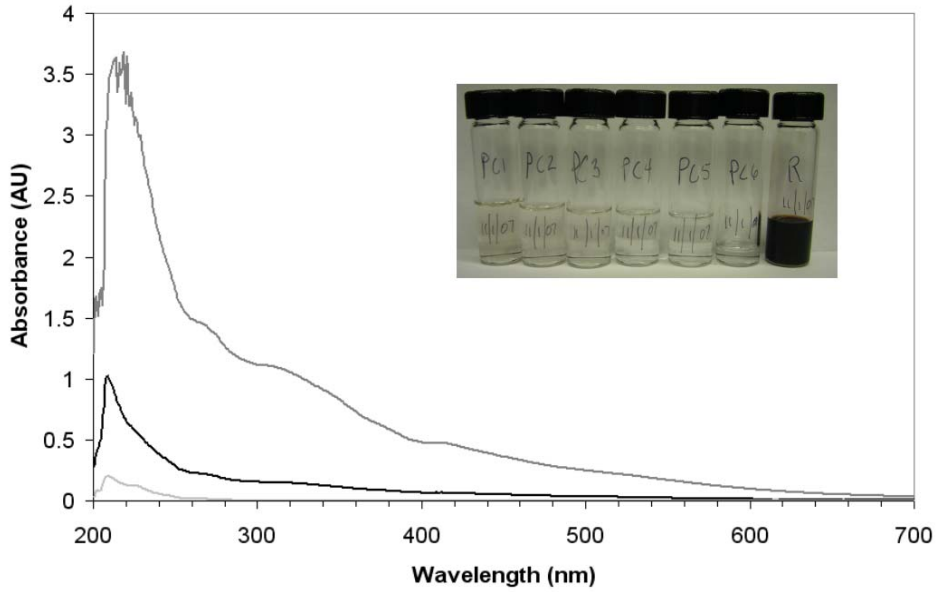

Figure 36: Diafiltration of post-synthetic Au_{11}, Trial 7, Step 4. Conditions: P = 1.4 bar, V_f = 25 mL, V_r = 2.5 mL. Legend: black = feed; dark gray = retentate; light gray = permeate. All samples were diluted by 100x to allow absorbance measurements. Rejection = 0.994 averaged over 410-420 nm. Photo insert: undiluted permeates.

The PPh_3 concentration decreases with each subsequent step (Figs. 37 and 38). A summary of Trial 7 is given in Figure 39 showing the final retentate, along with the original feed and the 0.1 g/L Au_{11} standard for comparison. In contrast to Trial 6, the post-synthetic feed spectrum is much different in shape compared to that of the standard and lower in magnitude than the feed in Trial 6 indicating a lower concentration of Au_{11}. The PPh_3 triad is seen again in the feed at the expected concentration of ~1 g/L. The final retentate bears a close resemblance to the feed and has a PPh_3 concentration comparable to that of the standard but does not show any improvement in the Au_{11} indicative peaks.

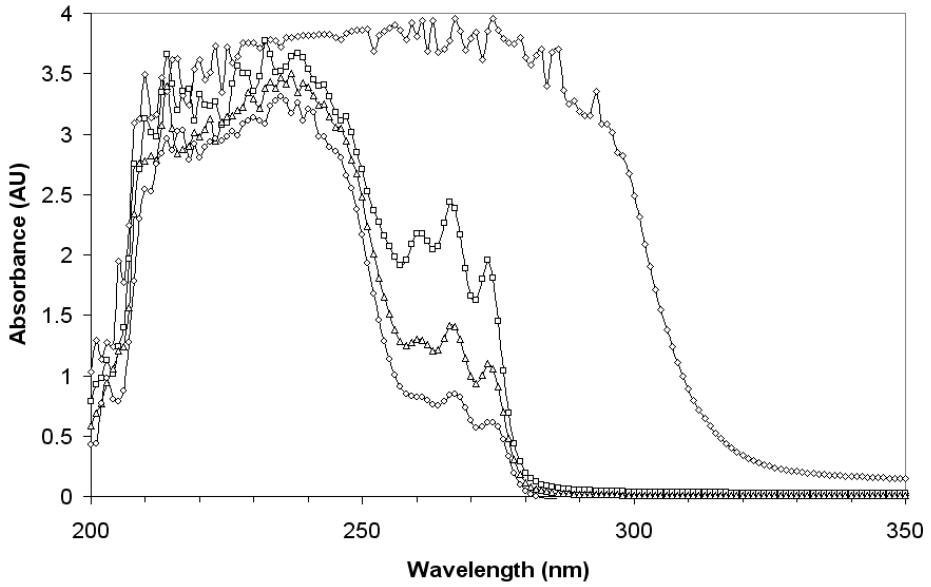

Figure 37: Permeates of the Trial 7 diafiltration of post-synthetic Au_{11}. Legend: ◇ = Step 1; □= Step 2; △= Step 3; ○= Step 4. All permeates are shown at original, undiluted concentration. This shows a decrease in the concentration of PPh_3 for each step.

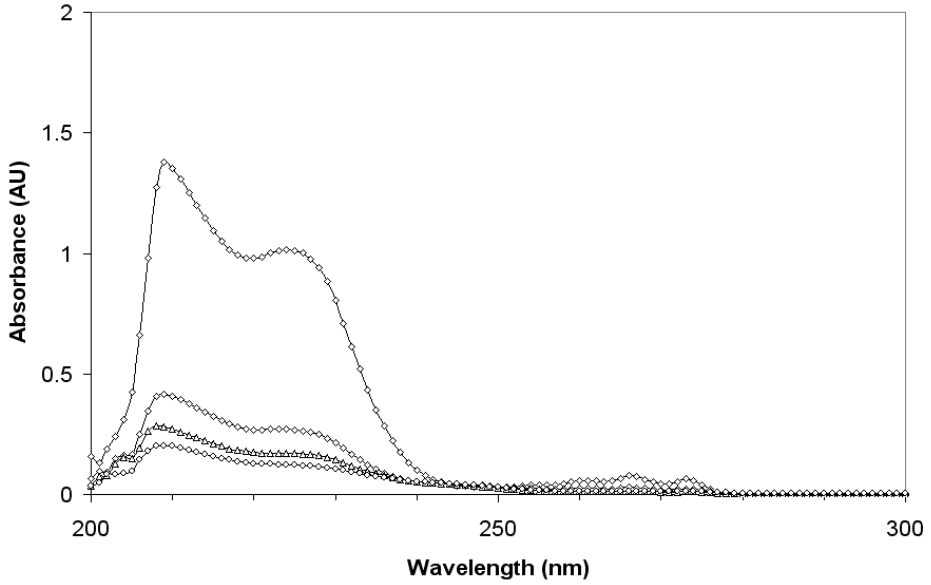

Figure 38: Diluted permeates of the Trial 7 diafiltration of post-synthetic Au_{11}. Legend: ◇ = Step 1; □ = Step 2; △ = Step 3; ○ = Step 4. All permeates are diluted with 50% THF by 100x. This shows a decrease in the concentration of PPh_3 for each step.

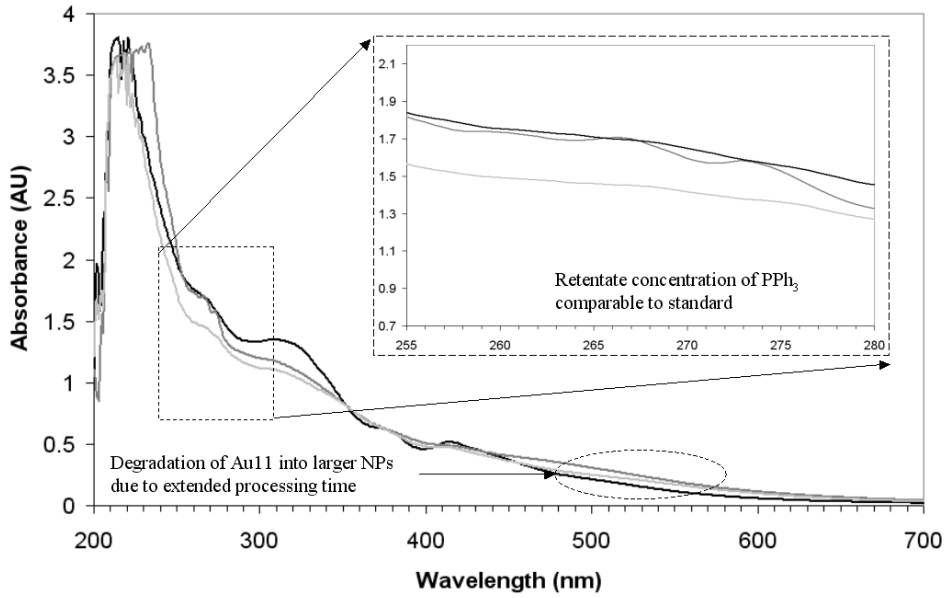

Figure 39: Trial 7 diafiltration of post-synthetic Au_{11} Summary. Legend: black = Au_{11} standard, 0.1 g/L; dark gray = post-synthetic Au_{11}, 100x dilution; light gray = retentate after four diafiltration steps, 100x dilution.

This demonstrates that PPh_3 was, as in the previous trial, removed from the product stream to a point comparable to conventional filtration. However, little can be said about Au_{11} directly in the absence of the expected spectral shape. It can be said that the diafiltration method retained a broadly absorbing species, similar to Au_{11}, which was present in this feed.

As before, the loss of Au_{11} product is apparent. Again, most of the loss is attributable to fluid handling such as rinsing and sampling. In this trial, the absorbance magnitudes of the feed and the final retentate are comparable indicating that about 25% of the product remains. This increase in performance over Trial 6 is most likely attributable to a shorter process time of

three days contributing to a decrease in plating out of the gold. Evidence of this is seen in comparing the vials of the two trials in which the retentate was stored overnight (Fig. 32). However, Au_{11} was likely still lost to some extent in the formation of larger gold nanoparticles as evidenced by the decrease in absorbance in the low 300 nm range and the coinciding increase in absorbance in the low 500 nm range.

4.3.2.3 Trial 8: Rejection of Triphenyphosphine

Following Trial 7, the MTF was characterized with 1g/L PPh_3, prepared fresh from solid stock, in an attempt to better assess if the rejection of PPh_3 had been effected by the exposure to the post-synthetic Au_{11} feed. Conditions were V_f = 25 mL, V_r = 2.5 mL, and P = 1.4.

A surprising result was the presence of a colored retentate originating from a colorless feed (Fig. 40). The color was due to gold nanoparticle species as evidenced by gold plating on the vial used to store the retentate and by the indicative absorbance peaks in the low 400 nm and low 500 nm ranges. These nanoparticles must have been immobilized in the upper channel of the MTF during previous tests and released during this filtration perhaps upon exposure to relatively high concentrations of PPh_3. A zero absorbance signal in the undiluted permeate from 350-700 nm indicates that no gold was detectable.

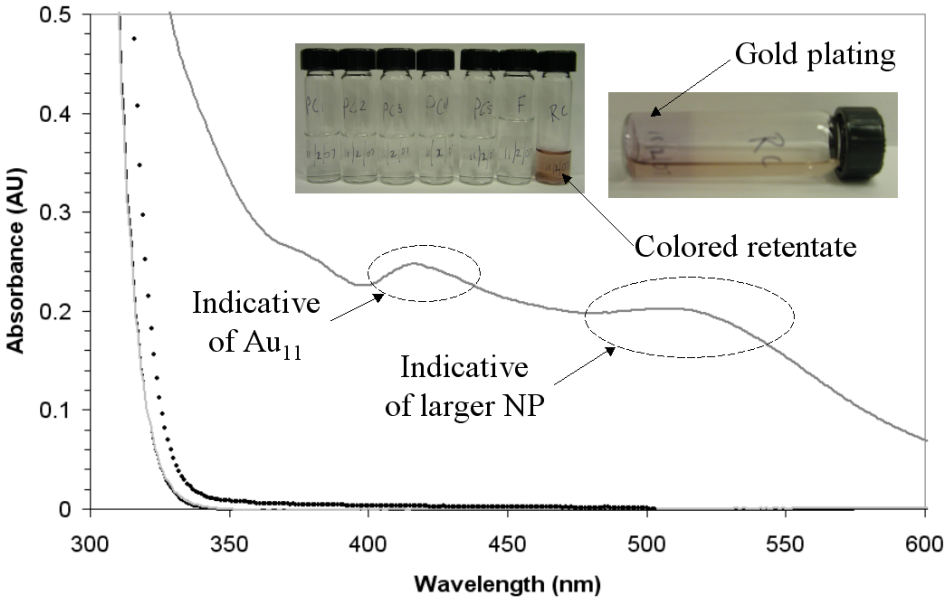

Figure 40: Comparison of the filtration of PPh_3 before and after the filtration of post-synthetic Au_{11}. Legend: dark gray = retentate after Au_{11} filtration; dotted = retentate before Au_{11} filtration; black = 1.0 g/L PPh_3 feed; light gray = permeate. Inset photos show the unexpected colored retentate and evidence of gold plating on the bottom of the retentate vial following 24 hours of refrigerated storage.

The diluted retentate, feed, final permeate and rejection are shown in Figure 41. A 0.47 rejection, calculated from the absorbance values at 225 nm, is higher than expected in comparison to the 0.12 measured under the same conditions in Trial 5 prior to post-synthetic testing. The retentate signal might be artificially high due to the presence of the gold species, leading to an error in the rejection calculation. This suspicion is not borne out with a rough back-calculation estimating a retentate signal of 1.88, comparable to the 1.66 measured at 225 nm, suggesting that the 0.47 rejection is indeed accurate (using Equations 3a-c; the permeate and feed signals measured at 225 nm of 0.882 and 0.982, respectively; and $V_f = 25$ mL, $V_r = 2.5$, as stated above). In

any case, mass transport of PPh_3 is evident within the range observed in previous trials.

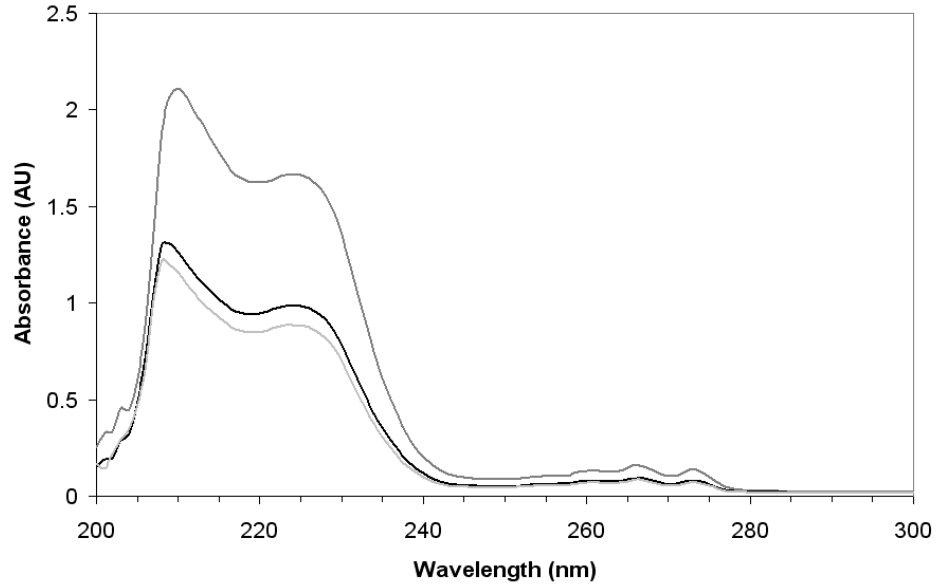

Figure 41: Performance of the MTF following Trial 7 diafiltration of post-synthetic Au_{11}. Legend: dark gray = retentate; black = 1.0 g/L PPh_3 feed; light gray = permeate. The retentate, feed and permeate were diluted 100x in order to facilitate UV-vis absorbance measurements.

4.3.2.4 Trial 9: Post-Synthetic Au_{11}

Several parameters were changed in the Trial 9 in an attempt to increase the recovery of the Au_{11} product and the elimination of PPh_3 from the product stream. First of all, the pressure was increased from 1.4 bar to 6.9 bar thereby increasing the transmembrane flux and decreasing the overall process time to less than two days in an effort to minimize the decomposition of Au_{11}. Secondly, all feed volumes were increased to 50 mL thereby setting $V_f/V_r = 20$ for all the steps in an effort to increase the mass transport of PPh_3 across the membrane (Eq. 3). Thirdly, an effort was made to reduce sampling and

handling losses. To reduce sampling losses only two 100 μL samples were taken from the Au_{11} product stream: (1) from the feed of Step 1 and (2) from the retentate of Step 4. To reduce handling losses, the retentates of Steps 1-3 were flushed back into the feed reservoir with 47.5 mL of 50% THF in order to form the feed Steps 2-4. This recovered any product remaining in the feed reservoir and upper channel. Ironically, about half of the post-synthetic sample was accidentally spilled onto the floor prior to the trial and was not recovered.

The permeates show significantly greater concentrations of Au_{11} as compared to those of the previous two trials indicating a decrease in rejection instead of the anticipated increase (Fig. 42). Another unexpected drop in rejection is apparent between Steps 2 and 3. This coincides with an overnight storage of the MTF with the upper channel filled with 50% THF so that the membrane would not dry out. Increases in rejection over the course of each step are once again apparent, especially in Steps 1 and 3.

These three observations are thought to be further evidence of adsorption of gold nanoparticles to the active membrane. Removal of the adsorbed particles in the previous trial could have resulted in the overall decrease in rejection observed in this trial as compared to prior trials. Adsorption of particles onto the membrane during the trial could explain the increases in rejection within each step seen in this and previous trials. The decrease in rejection between

Steps 2 and 3 could be due to desorption of particles from the membrane into the 50% THF storage solution.

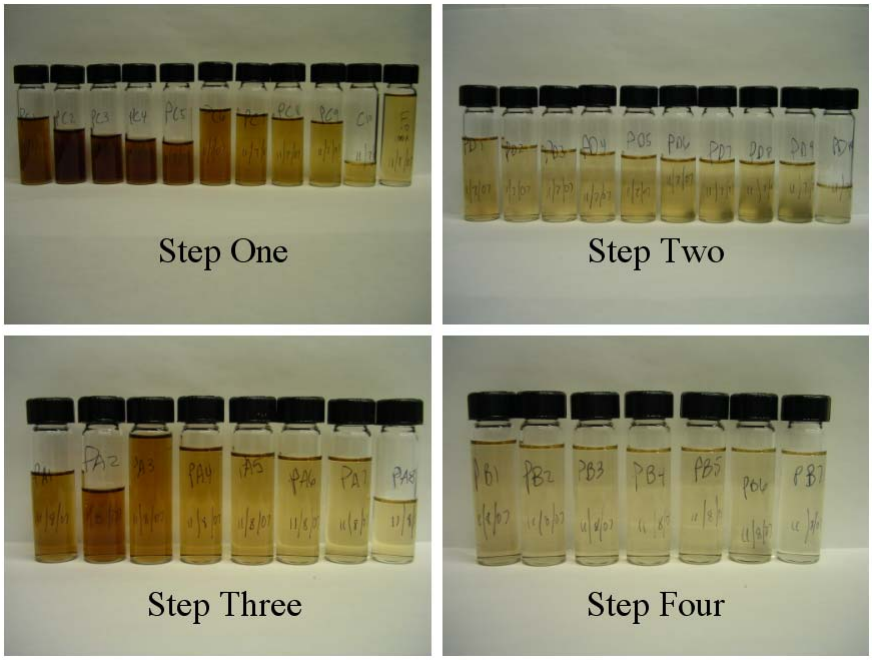

Figure 42: Undiluted permeates of the Trial 9 diafiltration of post-synthetic Au_{11} purification.

The rejection of PPh_3 seems to have not been significantly affected. The UV absorbance spectra of the last permeates of each of the four steps are shown in Figure 43. The spectrum of the Step 1 permeate shows the indicative PPh_3 triad, in the 250-280 region, riding on the slope provided by the Au_{11} signal, evidenced by the absorbance maximum around 310 nm. This relative magnitude appears comparable to that of the 0.1 g/L triad of the PPh_3 standard (Fig.16). The PPh_3 concentration in the *feed* should be about 0.1 g/L since it was originally ~1.0 g/L and has been diluted by 10x as compared with the initial feed of Trials 6 and 7 (2x by dumping half of the post-synthetic feed on

the floor and 5x by diluting the remaining feed to 50 mL prior to Step 1). A *permeate* concentration comparable to a *feed* concentration is indicative of low rejection. The remaining pemeates show an expected decrease in the concentration of PPh_3 over subsequent steps.

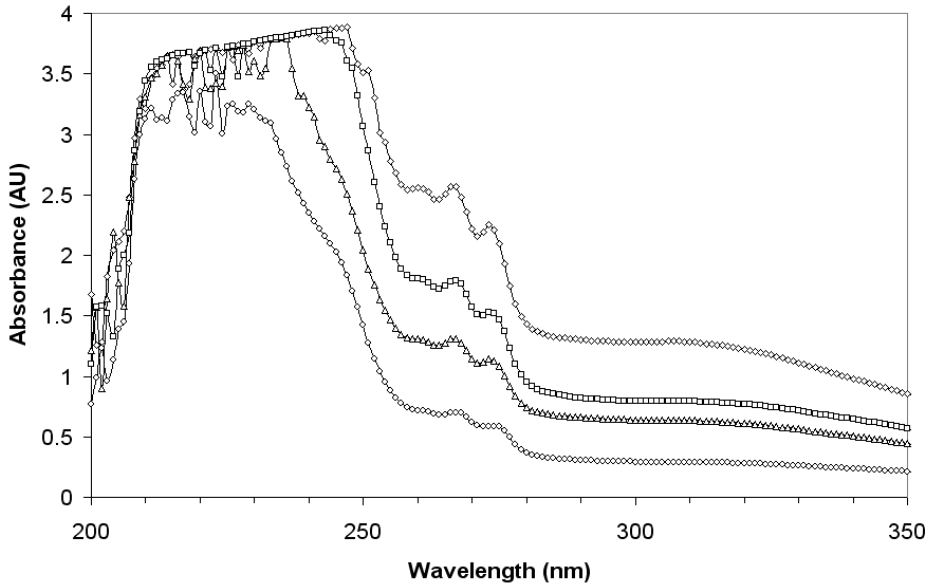

Figure 43: Permeates of the Trial 9 diafiltration of post-synthetic Au_{11}. Legend: ◇ = Step 1; □= Step 2; △= Step 3; ○= Step 4. All permeates are shown at original, undiluted concentration. This shows a decrease in the concentration of PPh_3 for each step.

A summary of Trial 8 is given in Figure 44 showing the final retentate, along with the original feed and the 0.1 g/L Au_{11} standard for comparison. The post-synthetic feed spectrum has the shape of the standard but still lacking in magnitude as compared to the feed in Trial 6 indicating a diminished concentration of Au_{11}. The final retentate shows removal of PPh_3 to conventional standards but no improvement in the Au_{11} indicative peaks.

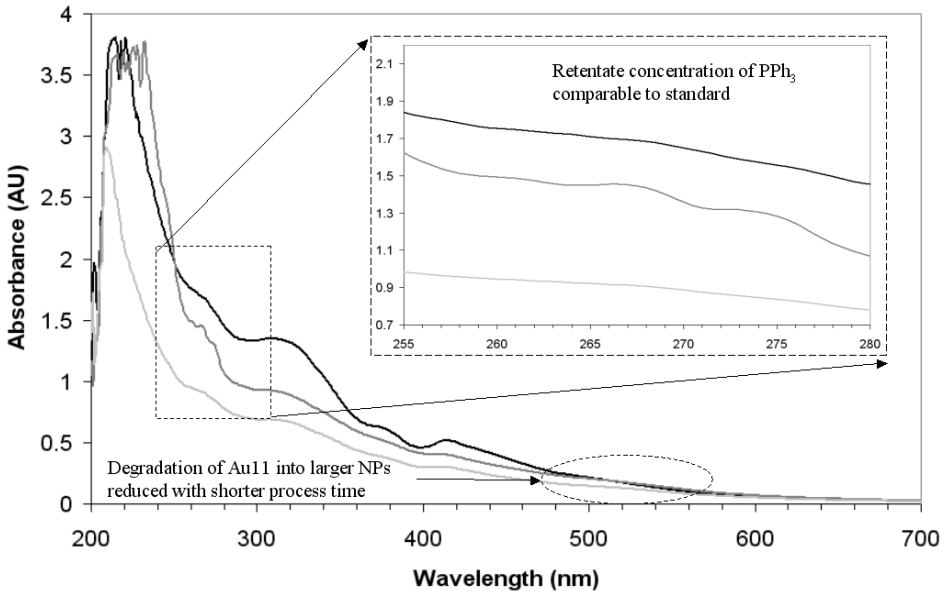

Figure 44: Trial 9 diafiltration of post-synthetic Au_{11} Summary. Legend: black = Au_{11} standard, 0.1 g/L; dark gray = post-synthetic Au_{11}, 100x dilution; light gray = retentate after four diafiltration steps, 100x dilution.

As before, the loss of Au_{11} product is apparent, mostly due to a decrease in the rejection especially in the first halves of Steps 1 and 3. The magnitude of the final retentate is about 75% that of the feed indicating that ~40% of the starting product remains (taking into account the diminished original feed volume of ~5 mL). This increase in performance over Trials 6 and 7 is attributable to greatly reduced sampling and handling losses. A back calculation using Eq.3, $V_f/V_r = 20$ and $m_r/m_f = 40\%$ reveals that this trial had an estimated average rejection of 0.99. There was also no evidence of gold plating out this time along with no evidence of the formation of larger nanoparticles.

4.3.3 Overall Permeance

The permeances in the MTF were closely correlated with feed concentration (Fig. 45). Any data point not otherwise labeled is a 50% THF feed for flushing the membrane.

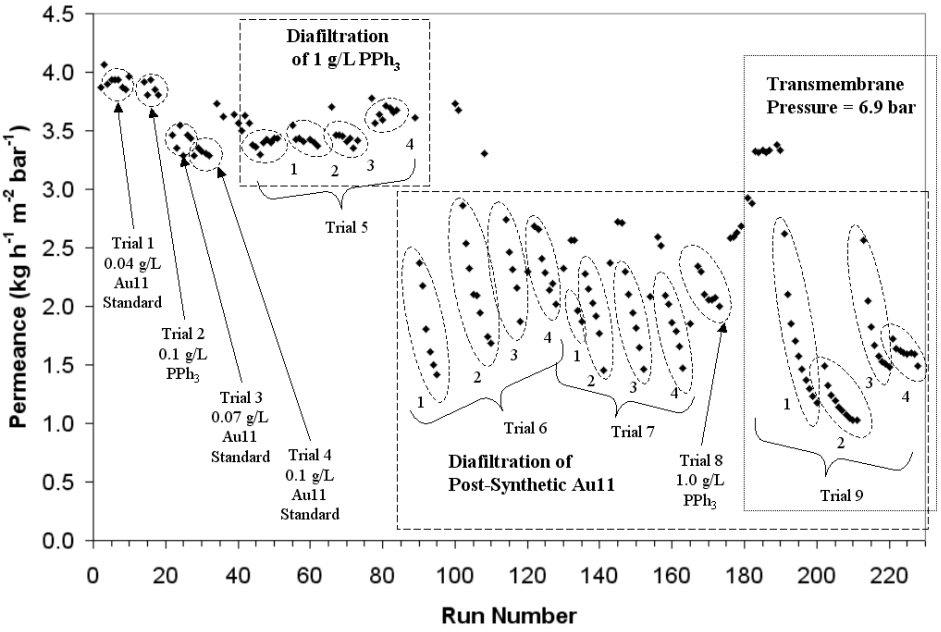

Figure 45: Permeance in the MTF for post-synthetic Au_{11} purification. All unlabeled data points are for 50% v/v THF/EtOH. All transmembrane pressures are 1.4 bar with the exception of the last set of runs at 6.9 bar.

The permeance decreases as the concentration of the Au_{11} standard is increased in Trials 1, 3 and 4; increases over the course of Trial 5 as the concentration of PPh_3 decreases; and takes a sharp decline at the beginning of Trial 6 when the feed is changed to post-synthetic Au_{11} due to higher concentration of nanoparticles. Periodic behavior then dominates the diafiltration of post-synthetic Au_{11} as each step begins with a diluted feed that becomes a more

concentrated retentate. The permeate recovers to previous levels following the unexpected appearance of gold species in the retentate in Trial 8 as 50% THF is flushed through the membrane. With increased pressure on a post-synthetic feed the permeance dips to the lowest levels in the testing and appears to "bottom out" as the data trends curl to the right. This happens to be near the value of 0.5 L m^{-2} h^{-1} bar^{-1} reported by the manufacturer.

4.4 Discussion

The MTF can be used to purify and concentrate a post-synthetic Au_{11} product stream, retaining Au_{11} and removing the PPh_3 byproduct, without the use of additional solvents or large amounts of energy. The permeance varies with concentration but only by a factor of four over the entire range of concentrations and recovers when not actively filtering. Purity of the filtered Au_{11} product is comparable to that of the conventionally purified standard. Process times on the order of one day are needed in order to avoid product loss due to plating out and agglomeration into larger nanoparticles.

Adsorption of gold nanoparticle species onto the membrane during processing is suspected for several reasons. First of all, the permeance of PPh_3 prior to post-synthetic trials was greater than that immediately following post-synthetic trials. Secondly, the retentate of the PPh_3 filtration in Trial 8 contained gold nanoparticles that originated from somewhere within the upper channel of the

MTF, possibly from the surface of the membrane. Thirdly, the permeance recovered immediately after the gold nanoparticles were removed from the upper channel.

This adsorption might have an overall *positive* effect on the performance of the membrane. Trials 6 and 7 were conducted under identical initial conditions and comparable feed concentrations. However, the performance of the membrane improved in the seventh trial as compared to the sixth in regard to the permeate color and calculated rejections. The performance of the membrane decreased in Trial 9 as compared to the Trial 6 and 7 *after* removal of the gold nanoparticles from the upper channel.

Unfortunately, several variables were changed in the Trial 9 making it more difficult to draw the conclusion that nanoparticle adhesion to the membrane surface is the dominating factor in performance. The most significant change in the conditions of the ninth trial was the five-fold increase in transmembrane pressure. However, in nanofiltration, rejection is expected to *increase* with increased pressure.

Further analysis is necessary to determine the optimal parameters for post-synthetic Au_{11} purification. Perhaps a conditioning of the membrane is necessary to develop a thin layer of adhered gold nanoparticles onto the

surface of the membrane in order to achieve top performance. Future work is also needed to determine the fate and transport of the post-synthetic species that have not been identified and monitored in this work.

5 Conclusion

5.1 Survey of Results

A macroscale test fixture (MTF) and microfluidic nanofiltration module (MTF) have been designed, fabricated and demonstrated for post-synthetic purification of macromolecules and nanoparticles via organic solvent nanofiltration. The methods can scale to bench-top or industrial systems and the devices can be integrated with other microfluidic components within a nanofactory. Whenever possible the materials used were inexpensive, transmissive and able to be shaped and joined using existing methods. A novel method of transmission laser welding was developed to provide a gasketing weld between a nanofiltration membrane and hard-polymer substrate. Stable permeances were observed for the MNM and MTF that are in good agreement with those published in literature and claimed by the manufacturer.

Characterization with Rhodamine B showed the positive correlation of pressure and rejection expected for a nanofiltration membrane dominated by diffusive mass transport. This finding suggests that the system performance could be tuned for selectivity by adjusting the applied transmembrane pressure. Higher pressures could be applied when lower molecular weight cutoffs were desired while lower pressures could be applied for higher molecular weight cutoffs.

A molecular weight cutoff (MWCO) of 2.3 kDa was determined in the MNM using carboxyl-terminated half-generation polyamidoamine (PAMAM) dendrimers at concentrations of 1 g/L and transmembrane pressures of 1.4 bar. The MNM and MTF were found to be *compatible* with a mixture of methyl acrylate and carboxyl-terminated half-generation PAMAM dendrimers but *incompatible* with ethylene diamine and, by extension, amine-terminated full-generation PAMAM dendrimers. This finding, along with rejections < 0.99 for half-generations up to G3.5, severely limit the applicability of the MNM toward the post-synthetic purification of PAMAM dendrimers at the given test conditions.

The MNM and MTF were found to be compatible with the species anticipated in the post-synthetic gold-eleven (Au_{11}) product stream. However, the supply of MNMs was exhausted prior to testing with a real-world sample. Purification of a post-synthetic Au_{11} product stream via diafiltration was demonstrated in the MTF with high rejection of Au_{11} and low rejection of triphenylphosphine (PPh_3), the anticipated dominant byproduct. The resulting retentate was comparable in quality to that of conventionally purified Au_{11}. This diafiltration method realizes improvements over conventional purification by eliminating the need for additional solvents and significantly reducing the energy required.

5.2 Other Possible Applications

As an analytical tool, the MNM could serve as a front-end device for on-line sample preparation prior to chromatographic and/or electrophoretic separations on a chip. Possible applications include but are not limited to: (1) preconcentration of high molecular mass analytes in large-volume environmental samples in the field; (2) more rapid sample prep in the lab such as desalting of proteins or recovery of drugs from biological samples; and (3) fractionation of molecules in flowing product streams for automated process analyses.

5.3 Future Work

5.3.1 Microfluidic Nanofiltration Module (MNM)

The performance of the MNM is expected to improve with application of a sweep through the permeate channel in counter current flow. This is expected to (1) decrease the bulk concentration of all species in the permeate; (2) decrease the concentration of all species at the membrane/permeate boundary; and (3) increase the concentration gradient across the membrane. Removal of byproducts and excess reagents would be enhanced due to an increase in transmembrane concentration gradient and a predicted decrease in rejection.

The MNM was limited to a pressure of 1.4 bar due to failure observed at higher pressures. This was most likely a consequence of module fabrication since the membrane itself is normally operated at 30-60 bar and no leakage was observed in the MTF at pressures up to 6.9 bar. An observed outward bowing of the APET fluidic channels while under pressure resulted in an increase in the tensile forces at the gasketing weld line. The glass slab reinforcement was implemented in response to this observation. Future work will likely involve numbering up of the microfluidic modules in order to increase throughput. Efforts should be made to incorporate mechanical reinforcement of the broad channels such as stacking the laminae in such a way that the channels provide equal and opposite support for one another.

One recurring difficulty in welding the APET substrates was the evolution of bubbles within the weld seam thus producing possible passages for leakage and possibly weakening the weld. These bubbles might originate from water vapor coming out of the hygroscopic substrate upon heating. The heated water also leads to hydrolysis of the APET reducing the mechanical strength of the substrate itself. In the future, the APET substrates should be heated prior to welding in order to drive off the retained water an improve weld quality.

5.3.2 Macroscale Test Fixture (MTF)

A future macroscale test fixture (MTF), or its cross flow/counter flow analog, would benefit from construction using more chemically resistant materials. It has been demonstrated that transparency is no longer requisite. Stainless steel or aluminum would be prime candidates for structural components. Stainless steel sintered frits are also available to replace the glass frit currently in use. Gasketing could still be achieved with a PTFE encapsulated elastomeric O-ring or replaced with the far more expensive option of Kalrez.

5.3.3 Modeling

Future designs would benefit from computer modeling of the fluidic and mechanical systems involved. Computational fluid dynamics (CFD) software could be used to characterize pressure drops, velocity profiles and mass transport to predict system performance prior to fabrication. Those findings could be used to optimize parameters such as membrane surface area, channel height, channel length, and transmembrane pressure of a system design. Finite element analysis (FEA) software could be used to evaluate the material strengths of those same system designs to identify possible failure points.

Bibliography

1. Mulder, M.H.V., E.M. van Voorthuizen, and J.M.M. Peeters, *Membrane Characterization*, in *Nanofiltration: Principles and Applications*, A.I. Schaefer, A.G. Fane, and T.D. Waite, Editors. 2005, Elsevier Advanced Technology: Oxford. p. 89-117.
2. Livingston, A., et al., *Membrane Separation in Green Chemical Processing: Solvent Nanofiltration in Liquid Phase Organic Synthesis Reactions.* Ann NY Acad Sci, 2003. **984**(1): p. 123-141.
3. Jiang, Y., et al., *Integrated Plastic Microfluidic Devices with ESI-MS for Drug Screening and Residue Analysis.* Analytical Chemistry, 2001. **73**(9): p. 2048-2053.
4. Long, Z., et al., *Integration of nanoporous membranes for sample filtration/preconcentration in microchip electrophoresis.* Electrophoresis, 2006. **27**(24): p. 4927-4934.
5. Xu, X., et al., *Electrophoretic Analysis and Purification of Fluorescent Single-Walled Carbon Nanotube Fragments.* Journal of the American Chemical Society, 2004. **126**(40): p. 12736-12737.
6. Zhang, Y. and A.T. Timperman, *Integration of nanocapillary arrays into microfluidic devices for use as analyte concentrators.* Analyst, 2003. **128**(6): p. 537-542.
7. Metz, S., et al., *Polyimide microfluidic devices with integrated nanoporous filtration areas manufactured by micromachining and ion track technology.* Journal of Micromechanics and Microengineering, 2004. **14**(3): p. 324-331.
8. Jongyoon, H., F. Jianping, and S.R. B., *Molecular sieving using nanofilters: Past, present and future.* Lab on a chip, 2008. **8**(1): p. 23-33.
9. Wu, Z., et al., *Polymer microchips bonded by O2-plasma activation.* Electrophoresis, 2002. **23**(5): p. 782-790.
10. Roberts, M.A., et al., *UV Laser Machined Polymer Substrates for the Development of Microdiagnostic Systems.* Analytical Chemistry, 1997. **69**(11): p. 2035-2042.
11. Rundel, J.T., B.K. Paul, and V.T. Remcho, *Organic solvent nanofiltration for microfluidic purification of poly(amidoamine) dendrimers.* Journal of Chromatography, A, 2007. **1162**(2): p. 167-174.
12. *The Technology Roadmap for Productive Nanosystems*. 2007 [cited December 24, 2007]; Available from: http://www.foresight.org/roadmaps/Roadmap2007_main.pdf.
13. Kockmann, N., et al., *Simulation and characterization of microreactors for aerosol generation.* Microfluidics and Nanofluidics, 2007. **3**(5): p. 581-589.

14. Koehler, J.M., et al., *Formation of Au/Ag nanoparticles in a two step micro flow-through process.* Chemical Engineering & Technology, 2007. **30**(3): p. 347-354.
15. Koehler, J.M., J. Wagner, and J. Albert, *Formation of isolated and clustered Au nanoparticles in the presence of polyelectrolyte molecules using a flow-through Si chip reactor.* Journal of Materials Chemistry, 2005. **15**(19): p. 1924-1930.
16. Mugdur, P.H., et al., *A Comparison of Chemical Bath Deposition of CdS from a Batch Reactor and a Continuous-Flow Microreactor.* Journal of the Electrochemical Society, 2007. **154**(9): p. D482-D488.
17. Sounart, T.L., et al., *Spatially-resolved analysis of nanoparticle nucleation and growth in a microfluidic reactor.* Lab on a Chip, 2007. **7**(7): p. 908-915.
18. Wagner, J. and J.M. Koehler, *Continuous Synthesis of Gold Nanoparticles in a Microreactor.* Nano Letters, 2005. **5**(4): p. 685-691.
19. Wagner, J., T.R. Tshikhudo, and J.M. Koehler, *Microfluidic generation of metal nanoparticles by borohydride reduction.* Chemical Engineering Journal, 2008. **135(Suppl. 1)**: p. S104-S109.
20. Zhao, H., et al., *Controlled liquid antisolvent precipitation of hydrophobic pharmaceutical nanoparticles in a microchannel reactor.* Industrial & Engineering Chemistry Research, 2007. **46**(24): p. 8229-8235.
21. Zinoveva, S., et al., *The wet chemical synthesis of Co nanoparticles in a microreactor system: A time-resolved investigation by X-ray absorption spectroscopy.* Nuclear Instruments & Methods in Physics Research, Section A: Accelerators, Spectrometers, Detectors, and Associated Equipment, 2007. **582**(1): p. 239-241.
22. Liu, S. and C.-h. Chang, *High rate convergent synthesis and deposition of polyamide dendrimers using a continuous-flow microreactor.* Chemical Engineering & Technology, 2007. **30**(3): p. 334-340.
23. Wilms, D., et al., *Synthesis of hyperbranched polyglycerol in a continuous flow microreactor.* Chemical Engineering & Technology, 2007. **30**(11): p. 1519-1524.
24. Carrel, F.R., et al., *Oligosaccharide Synthesis in Microreactors.* Organic Letters, 2007. **9**(12): p. 2285-2288.
25. Becht, S., et al., *Micro process technology as a means of process intensification.* Chemical Engineering & Technology, 2007. **30**(3): p. 295-299.
26. Krishnadasan, S., et al., *Intelligent routes to the controlled synthesis of nanoparticles.* Lab on a Chip, 2007. **7**(11): p. 1434-1441.
27. McKenzie, L.C. and J.E. Hutchison, *Green nanoscience.* Chimica Oggi, 2004. **22**(9): p. 30-33.
28. Dahl, J.A., B.L.S. Maddux, and J.E. Hutchison, *Toward greener nanosynthesis.* Chemical reviews, 2007. **107**(6): p. 2228-2269.

29. Chattopadhyay, D., et al., *Length separation of zwitterion-functionalized single wall carbon nanotubes by GPC.* Journal of the American Chemical Society, 2002. **124**(5): p. 728-729.
30. Niyogi, S., et al., *Chromatographic Purification of Soluble Single-Walled Carbon Nanotubes (s-SWNTs).* Journal of the American Chemical Society, 2001. **123**(4): p. 733-734.
31. Zhao, B., et al., *Chromatographic purification and properties of soluble single-walled carbon nanotubes.* Journal of the American Chemical Society, 2001. **123**(47): p. 11673-11677.
32. Krueger, K.M., et al., *Characterization of Nanocrystalline CdSe by Size Exclusion Chromatography.* Analytical Chemistry, 2005. **77**(11): p. 3511-3515.
33. Al-Somali, A.M., et al., *Recycling Size Exclusion Chromatography for the Analysis and Separation of Nanocrystalline Gold.* Analytical Chemistry, 2004. **76**(19): p. 5903-5910.
34. Siebrands, T., et al., *Steric exclusion chromatography of nanometer-sized gold particles.* Langmuir, 1993. **9**(9): p. 2297-2300.
35. Wei, G.-T. and F.-K. Liu, *Separation of nanometer gold particles by size exclusion chromatography.* Journal of Chromatography, A, 1999. **836**(2): p. 253-260.
36. Wei, G.-T., F.-K. Liu, and C.R.C. Wang, *Shape separation of nanometer gold particles by size-exclusion chromatography.* Analytical Chemistry, 1999. **71**(11): p. 2085-2091.
37. Schnabel, U., C.-H. Fischer, and E. Kenndler, *Characterization of colloidal gold nanoparticles according to size by capillary zone electrophoresis.* Journal of Microcolumn Separations, 1997. **9**(7): p. 529-534.
38. Jimenez, V.L., et al., *HPLC of monolayer-protected gold nanoclusters.* Analytical Chemistry, 2003. **75**(2): p. 199-206.
39. Wilcoxon, J.P., J.E. Martin, and P. Provencio, *Size distributions of gold nanoclusters studied by liquid chromatography.* Langmuir, 2000. **16**(25): p. 9912-9920.
40. Bos, W., et al., *Separation of cationic metal cluster compounds by reversed phase HPLC.* Inorganic Chemistry, 1988. **27**(5): p. 948-951.
41. Jahanshahi, M., Z. Zhang, and A. Lyddiatt, *Subtractive chromatography for purification and recovery of nano-bioproducts.* IEE proceedings. Nanobiotechnology, 2005. **152**(3): p. 121-126.
42. Machado, D.R., D. Hasson, and R. Semiat, *Effect of solvent properties on permeate flow through nanofiltration membranes. Part I: investigation of parameters affecting solvent flux.* Journal of Membrane Science, 1999. **163**(1): p. 93-102.
43. Silva, P., S. Han, and A.G. Livingston, *Solvent transport in organic solvent nanofiltration membranes.* Journal of Membrane Science, 2005. **262**(1-2): p. 49-59.

44. Koros, W.J., Y.H. Ma, and T. Shimidzu, *Terminology for membranes and membrane processes.* Pure and Applied Chemistry, 1996. **68**(7): p. 1479-1489.
45. Linder, C. and O. Kedem, *History of Nanofiltration Membranes 1960 to 1990*, in *Nanofiltration: Principles and Applications*, A.I. Schaefer, A.G. Fane, and T.D. Waite, Editors. 2005, Elsevier Advanced Technology: Oxford. p. 5-31.
46. Schaefer, A.I., A.G. Fane, and T.D. Waite, *Introduction*, in *Nanofiltration: Principles and Applications*, A.I. Schaefer, A.G. Fane, and T.D. Waite, Editors. 2005, Elsevier Advanced Technology: Oxford. p. 1-4.
47. Bowen, W.R. and J.S. Welfoot, *Modelling the Performance of Nanofiltration Membranes*, in *Nanofiltration: Principles and Applications*, A.I. Schaefer, A.G. Fane, and T.D. Waite, Editors. 2005, Elsevier Advanced Technology: Oxford. p. 119-146.
48. Peeva, L.G., et al., *Effect of concentration polarisation and osmotic pressure on flux in organic solvent nanofiltration.* Journal of Membrane Science, 2004. **236**(1-2): p. 121-136.
49. Dalwadi, G., H.A.E. Benson, and Y. Chen, *Comparison of Diafiltration and Tangential Flow Filtration for Purification of Nanoparticle Suspensions.* Pharmaceutical Research, 2005. **22**(12): p. 2152-2162.
50. Huang, L., et al., *Separation and purification of nano-Al13 by UF method.* Colloids and Surfaces, A: Physicochemical and Engineering Aspects, 2006. **275**: p. 1-3.
51. Sweeney, S.F., G.H. Woehrle, and J.E. Hutchison, *Rapid Purification and Size Separation of Gold Nanoparticles via Diafiltration.* Journal of the American Chemical Society, 2006. **128**(10): p. 3190-3197.
52. Tishchenko, G., et al., *Ultrafiltration and microfiltration membranes in latex purification by diafiltration with suction.* Separation and Purification Technology, 2003. **30**(1): p. 57-68.
53. Tishchenko, G., et al., *Purification of polymer nanoparticles by diafiltration with polysulfone/hydrophilic polymer blend membranes.* Separation and Purification Technology, 2001. **22 and 23**(1-3): p. 403-415.
54. Akthakul, A., et al., *Size fractionation of metal nanoparticles by membrane filtration.* Advanced Materials, 2005. **17**(5): p. 532-535.
55. Jenkins, A.D., et al., *Glossary of basic terms in polymer science.* Pure and Applied Chemistry, 1996. **68**(12): p. 2287-2311.
56. Peterson, J., et al., *Synthesis and CZE analysis of PAMAM dendrimers with an ethylenediamine core.* Proceedings of the Estonian Academy of Sciences, Chemistry, 2001. **50**(3): p. 156-166.
57. Tomalia, D.A., et al., *A new class of polymers: starburst-dendritic macromolecules.* Polymer Journal, 1985. **17**(1): p. 117-132.

58. McNulty, J. and Y. Zhou, *A highly efficient general synthesis of phosphine-borane complexes.* Tetrahedron Letters, 2004. **45**(2): p. 407-409.
59. Sekulic, J., J.E. ten Elshof, and D.H.A. Blank, *Synthesis and characterization of microporous titania membranes.* Journal of Sol-Gel Science and Technology, 2004. **31**(1/2/3): p. 201-204.
60. Puhlfurss, P., A. Voigt, and R.M. Weber, M., *Microporous TiO2 membranes with a cut off <500 Da.* Journal of Membrane Science, 2000. **174**(1): p. 123-133.
61. Van Gestel, T., et al., *ZrO2 and TiO2 membranes for nanofiltration and pervaporation.* Journal of Membrane Science, 2006. **284**(1+2): p. 128-136.
62. Voigt, I., P. Puhlfurss, and J. Topfer, *Preparation and characterization of microporous TiO2 membranes.* Key Engineering Materials, 1997. **132-136**: p. 1735-1737.
63. Voigt, I., *Nanofiltration with ceramic membranes.* Chemie Ingenieur Technik, 2005. **77**(5): p. 559-564.
64. Bartlett, P.A., B. Bauer, and S.J. Singer, *Synthesis of water-soluble undecagold cluster compounds of potential importance in electron microscopic and other studies of biological systems.* Journal of the American Chemical Society, 1978. **100**(16): p. 5085-5089.

Appendicies

Appendix A: Material Compatibility Data

Table 3: Materials compatibility gravimetric analyis. Polymer materials are given at the top of each column. Solvent environments are given at the beginning of each row. Values are % change in mass of the polymer material after 24 hours exposure to the solvent environment, rinsing with methanol or ethanol and exposure to a rough vacuum for 10 minutes.

	SMA	SMB	APET	PEEK	EPDM	PSU	PTFE	PC	PDMS	PET	PETG	PMMA	PVC	PEI	Viton
100% EDA/MeOH	-100.00	-100.00	-100.00	0.11	2.78	3.08	0.00	-100.00	2.58	-26.05	-100.00	-100.00	14.77	-58.09	-100.00
10% EDA/MeOH	-33.54	-1.28	0.00	0.66	-2.70	1.44	0.02	-11.86	-0.89	0.07	0.21	3.45	0.10	7.57	-25.74
1% EDA/MeOH	4.41	-0.47	0.06	0.88	-9.21	1.69	0.02	-1.71	-0.93	-0.06	0.26	8.95	0.10	5.17	16.32
100% MA/MeOH	-34.51	1.55	6.34	15.80	-16.88	-100.00	0.08	20.25	-1.65	5.43	22.38	-100.00	63.44	17.04	12.44
10% MA/MeOH	-7.59	0.00	0.11	0.92	-5.26	1.88	0.03	1.60	-0.87	0.08	0.79	13.03	0.27	5.33	13.59
1% MA/MeOH	-6.10	-0.89	0.03	0.92	-7.89	1.79	0.02	1.30	-0.77	0.00	0.29	9.49	0.07	5.18	12.50
100% HAc/MeOH	-8.43	1.04	1.89	0.11	-2.82	0.28	0.08	1.48	0.18	0.72	-8.78	-100.00	0.25	0.00	35.47
10% HAc/MeOH	-0.64	-0.41	0.11	0.78	-4.00	1.58	0.03	1.20	-0.59	0.00	0.25	8.18	0.05	4.49	13.88
1% HAc/MeOH	-11.95	-0.85	0.06	0.85	-5.06	1.73	0.01	1.25	-0.78	-0.06	0.28	8.74	0.05	5.04	10.58
100% MeOH	-5.00	-0.78	0.06	0.79	-3.85	1.69	0.03	1.32	-0.77	0.00	0.27	8.93	0.03	4.83	10.29
100% THF	-22.16	2.00	14.74	18.04	-15.54	-100.00	----	----	----	----	----	----	----	----	----
90% THF/EtOH	----	----	12.72	21.03	----	-100.00	0.04	----	----	----	----	----	----	----	----
80% THF/EtOH	----	----	9.94	19.90	----	-100.00	0.05	----	----	----	----	----	----	----	----
70% THF/EtOH	----	----	7.20	19.18	----	-100.00	0.07	----	----	----	----	----	----	----	----
60% THF/EtOH	----	----	4.70	17.91	----	-100.00	-0.10	----	----	----	----	----	----	----	----
50% THF/EtOH	----	----	2.74	2.93	----	18.92	0.05	----	----	----	----	----	----	----	----
40% THF/EtOH	----	----	1.30	0.25	----	6.18	0.07	----	----	----	----	----	----	----	----
30% THF/EtOH	----	----	0.59	0.14	----	1.19	0.03	----	----	----	----	----	----	----	----
20% THF/EtOH	----	----	0.20	0.26	----	0.39	0.02	----	----	----	----	----	----	----	----
10% THF/EtOH	-20.43	1.61	0.03	0.29	-12.16	0.15	----	----	----	----	----	----	----	----	----
1% THF/EtOH	-19.65	2.50	-0.05	0.00	-9.33	0.10	----	----	----	----	----	----	----	----	----
100% DCM	-22.72	-2.67	23.09	17.11	-16.45	-100.00	----	----	----	----	----	----	----	----	----
10% DCM/EtOH	-19.45	4.39	0.37	0.47	-11.92	0.79	----	----	----	----	----	----	----	----	----
1% DCM/EtOH	-20.30	2.22	0.03	0.00	-10.07	0.15	----	----	----	----	----	----	----	----	----
100% EtOH	-19.62	1.54	-0.03	0.13	-9.03	0.15	----	----	----	----	----	----	----	----	----
Control	1.47	0.00	0.03	0.12	-1.39	0.03	0.01	0.05	-0.02	0.06	0.12	0.06	0.00	-0.24	0.49

Appendix B: Half-Generation PAMAM UV-vis Spectra

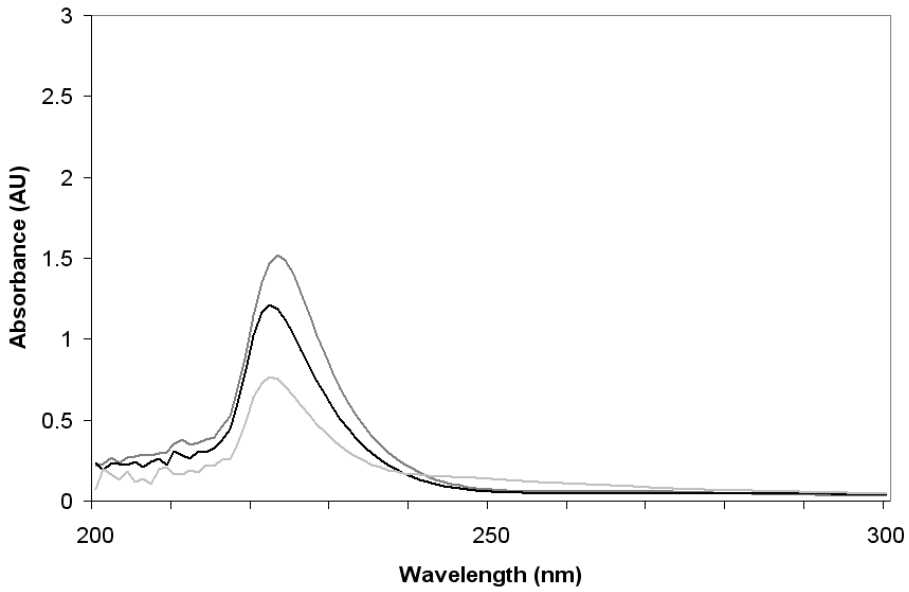

Figure 46: Generation -0.5 PAMAM dendrimer at 1.4 bar in the MNM, $V_f/V_r \sim 2$. Rejection average of 0.51 was calculated using data from 225-235 nm. Legend: black = feed; dark gray = retentate; light gray = permeate.

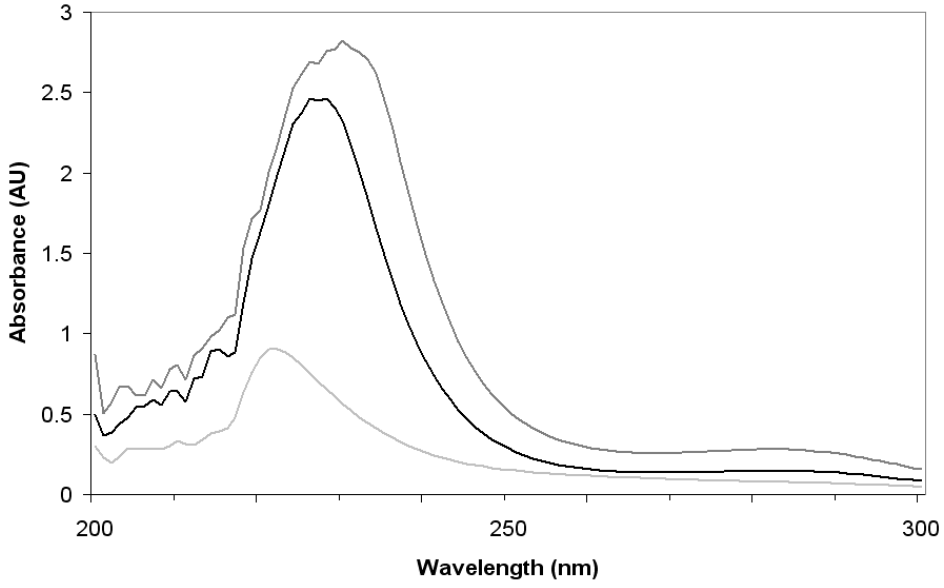

Figure 47: Generation 0.5 PAMAM dendrimer at 1.4 bar in the MNM, Vf/Vr ~ 2. Rejection average of 0.82 was calculated using data from 230-240 nm. Legend: black = feed; dark gray = retentate; light gray = permeate.

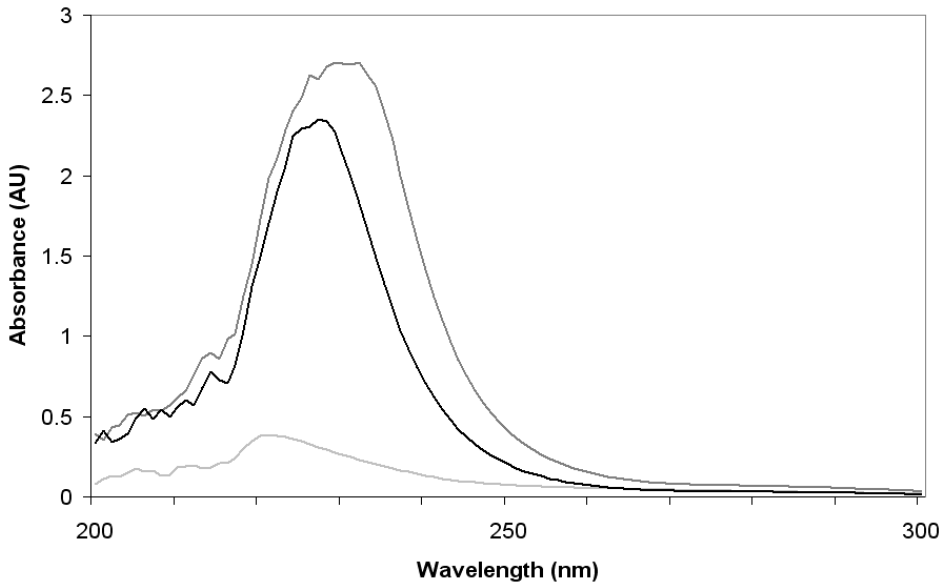

Figure 48: Generation 1.5 PAMAM dendrimer at 1.4 bar in the MNM, Vf/Vr ~ 2. Rejection average of 0.91 was calculated using data from 230-240 nm. Legend: black = feed; dark gray = retentate; light gray = permeate.

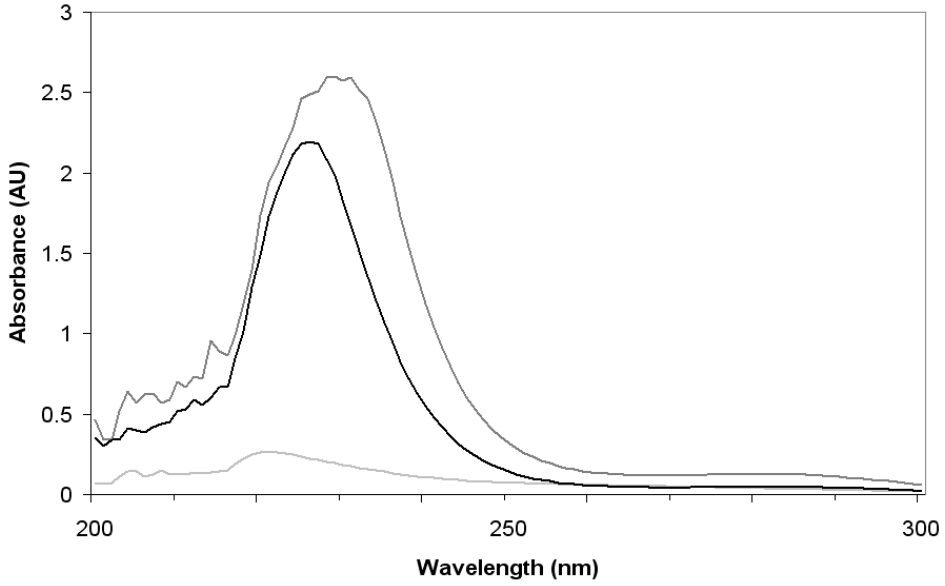

Figure 49: Generation 2.5 PAMAM dendrimer at 1.4 bar in the MNM, Vf/Vr ~ 2. Rejection average of 0.93 was calculated using data from 230-240 nm. Legend: black = feed; dark gray = retentate; light gray = permeate.

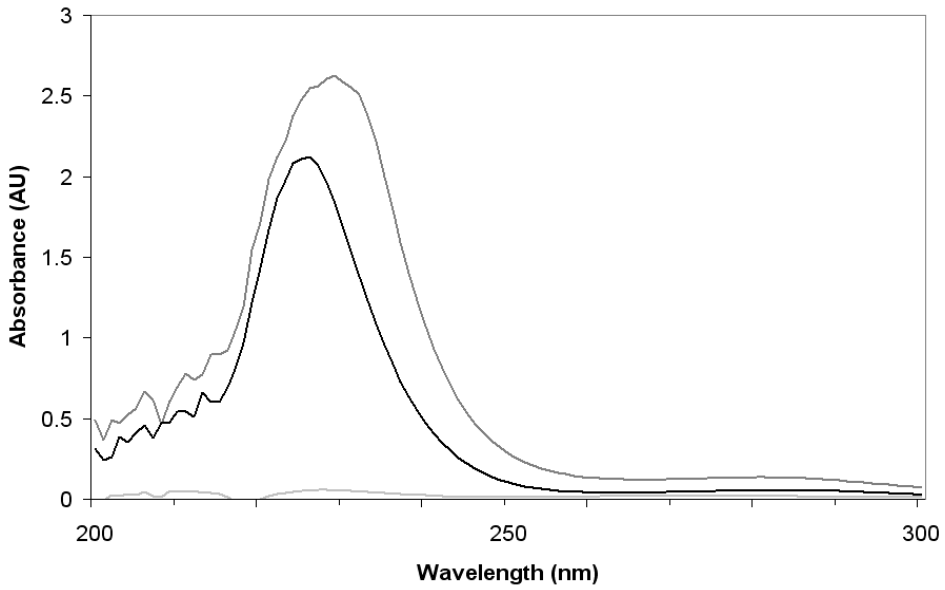

Figure 50: Generation 3.5 PAMAM dendrimer at 1.4 bar in the MNM, Vf/Vr ~ 2. Rejection average of 0.98 was calculated using data from 230-240 nm. Legend: black = feed; dark gray = retentate; light gray = permeate.